III-4

Surface, Interface and Thin Films

BL2A

Analysis of Electronic Structure of P3HT/ MoO_x Interface by Soft X-ray Absorption Spectroscopy

K. K. Okudaira[1], S. Yoshioka [2] and E. Kobayashi [3]

[1]*Graduate School of Science and Engineering, Chiba University, 1-33 Yayoi-cho Inage-ku, Chiba 263-8522, Japan*

[2]*Graduate School of Engineering, Kyushu University, 744 Motooka Nishi-ku Fukuoka 819-0395 Japan*

[3]*Kyushu Synchrotron Light Research Center, 8-7 Yayoigaoka, Tosu, Saga 841-0005, Japan*

1-33 Yayoi-cho Inage-ku, Chiba 263-8522, Japan

Organic thin-film solar cells are advantageous due to their low manufacturing costs; however, their low power conversion efficiency remains a challenge. One approach to improve efficiency is the introduction of metal oxides like MoO_3 as hole extraction layers or electron extraction layers between the organic layer and the two electrodes[1,2]. Furthermore, doping metal oxides to control their valence band structures and achieve appropriate energy alignment with the HOMO and LUMO of organic semiconductor layers is expected to lead to high-efficiency organic thin-film solar cells. However, when doped metal oxides are stacked with organic semiconductors, the formation of new interfacial electronic states is considered.

This study investigates the electronic states at the interface between molybdenum oxide, known as a hole extraction layer, and the organic film using soft X-ray absorption spectroscopy. To obtain insights into the buried interface, measurements utilizing the partial fluorescence yield method in soft X-ray absorption spectroscopy are effective. However, there are very few examples of incorporating such techniques into the development of organic thin-film solar cells

The sample are thin molybdenum oxide film fabricated on silicon using the RF magnetron sputtering method. One of the films was cleaned with neutral detergent, distilled water, acetone and UV ozone. P3HT was dissolved in chlorobenzene and deposited onto the thin film by spin coating. NEXAFS spectra of the MoO_x film using both total electron yield (TEY) and partial fluorescence yield (PFY) modes were measured at the beamline 2A of the UVSOR in the Institute of Molecular Science. For TEY, the drain current from the sample was measured. For PFY, fluorescence X-rays were collected using an energy dispersible silicon drift detector (SDD). All experiments were performed at room temperature.

Figure 1 shows the NEXAFS spectrum of P3HT/ MoO_x/Si thin film in PFY mode. The observed spectrum is considered to consist of two components, Peak A and Peak B[3]. Adsorbing P3HT onto the MoOx thin film resulted in Peak A becoming more intense than Peak B. This suggests that electronic states were generated at the interface between the organic film and the oxide film. Furthermore, when P3HT was adsorbed onto a cleaned thin film, the intensity ratio changed, indicating that surface treatment of the oxide film alters the interfacial electronic states. This finding implies the possibility of controlling interfacial electronic states.

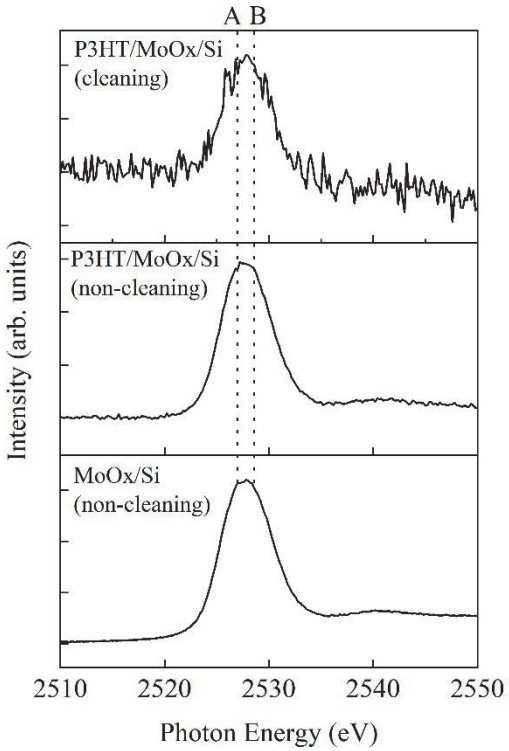

Fig. 1. Mo L-edge NEXAFS spectra of P3HT/MoO_x/Si thin film in PFY mode.

[1] D. W. Zhao *et al.*, Appl. Phys. Lett. **95** (2009) 153304.
[2] X. Hu, *et al*., J. Phys. Chem. C **118** (2014) 9930.
[3] A. Svyazhin *et al.*, Inorg. Chem. **61** (2022) 869.

BL3U

Oxygen K-Edge XAS-Evidenced Specific Hydrogen-Bonded Water inside Hydrophobic Single-Walled Carbon Nanotubes

Y. Kawamata[1], H. Otsuka[1], M. Nagasaka[2] and K. Kaneko[1,3]
[1]*Research Initiative for Supra-Materials Shinshu University, Nagano 380-8553, Japan*
[2]*Institute for Molecular Science, Okazaki 444-8585, Japan*
[3]*Institute for Aqua Regeneration Shinshu University, Nagano 380-8553, Japan*

Understanding the properties of hydrogen-bonded water molecules around functional groups on nanopores of hydrophobic carbon surfaces or biological substances is crucial. Although presence of only trace amounts of water molecules around functional groups on the hydrophobic surfaces are presumed, their effects should dominate the important phenomena such as water/ion permeation and energy storage in the electrical double layer [1, 2]. The direct observation of the hydrogen-bonded structure of only slight amount of water molecules inside nanopores is very challenging with conventional diffraction technique or Raman/IR spectroscopy because the background of solid hinder the signals of trace amount of water molecules. However, X-ray absorption spectroscopy (XAS) is a powerful tool for investigating the hydrogen-bonded structure of only a tiny water molecules inside nanopores, as it selectively detects specific atoms of interest [3]. In this study, we applied XAS to water molecules inside highly hydrophobic single-walled carbon nanotubes (SWCNTs). SWCNT has well-defined hydrophobic cylindrical nanopores, enabling to investigate the interactions between trace amount of water molecules and isolated functional groups on the graphene wall.

SWCNT with a diameter of 2 nm were purified by heating at 2073 K in vacuo for 3 hours, removing most of impurities. End-caps were removed by air oxidation at 823 K, enabling water molecules to access the SWCNT internal pores. The SWCNTs were dispersed in EtOH at a concentration of 0.01 wt%, and the dispersion was casted onto a SiN membrane with a thickness of 100 nm. EtOH were removed by vacuum evaporation at room temperature, producing a thin SWCNTs film with a thickness of 3 μm on the SiN membrane. The SWCNTs film on the SiN were placed in a XAS measurement chamber. O K-edge XAS spectrum of SWCNTs were measured in the range of 525 – 550 eV under water vapor introduced into the chamber via He bubbling of pure water.

Figure 1 shows the water adsorption isotherm of the SWCNTs. At the relative pressure (P/P_0) below 0.65, the water adsorbed amount is very small, suggesting the water exists as isolated water clusters inside SWCNT [4]. We carried out XAS measurement at $P/P_0 = 0.5$, where the water adsorbed amount is 20 mg g^{-1}, being only 4 % of the fractional filling against saturated adsorbed amount.

Figure 2 shows Oxygen K-edge XAS spectrum of SWCNTs. At $P/P_0 = 0$, two peaks are observed. A sharp peak at 532 eV and a broad peak at 539 eV are assigned to C=O and C-O, respectively. At $P/P_0 = 0.5$, the sharp peak at 532 eV broadens, evidencing the interactions between C=O and water molecules via hydrogen bonding. Furthermore, the intensity of the broad peak increases in the range of 536 – 542 eV due to the presence of water clusters. The increase of the broad peak intensity suggests that the intermolecular distance of water molecules fluctuates from the equilibrium distances. This is the direct evidence on water-surface oxygen groups interactions inside highly hydrophobic carbon spaces.

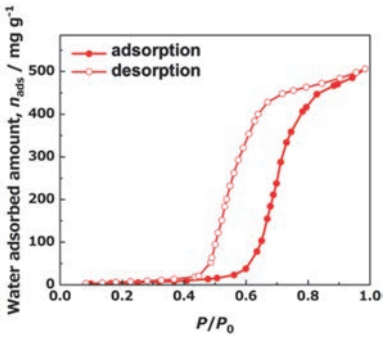

Fig. 1. Water adsorption isotherm of SWCNT at 298 K.

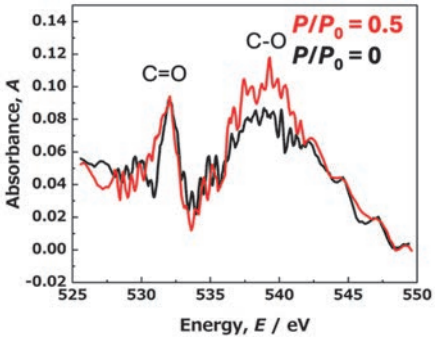

Fig. 2. O K-edge XAS spectrum of SWCNT.

[1] D. A. Doyle *et al.*, Science **280** (1998) 69.
[2] P. Simon and Y. Gogotsi, Nat. Mater. **19** (2020) 1151.
[3] T. Fransson *et al.*, Chem. Rev. **116** (2016) 7551.
[4] T. Ohba, H. Kanoh and K. Kaneko, J. Am. Chem. Soc. **126** (2004) 1560.

III-4

BL3U

Ionic Layers at the Electrode Interface of Ionic Liquids Studied Using Interface-Selective Soft X-ray Absorption Spectroscopy

K. Yamaguchi[1], T. Furuya[1], M. Nagasaka[2] and N. Nishi[1]
[1]*Graduate School of Engineering, Kyoto University, Kyoto 615-8510, Japan*
[2]*Institute for Molecular Science, Okazaki 444-8585, Japan*

Ionic liquids (ILs), which are entirely composed of cations and anions, are appealing materials as electrolytes for energy devices. In such devices, the electrochemical interface between ILs and electrodes is an electrochemical reaction field that strongly influences the local reaction rate and thereby the net ones such as charging speed for batteries. Thus, it is of crucial importance to study, and further control, the interfacial structure of ILs at the electrode interface. In the present study, we adopted soft X-ray absorption spectroscopy (XAS) to reveal the interfacial structure of ILs at the electrode interface in an interface-selective manner [1].

1-Butyl-1-methylpyrrolidinium bis(fluorosulfonyl) amide ([C4mpy$^+$][FSA$^-$]) that contained Li$^+$[FSA$^-$] at a concentration of 0.5 M was used as IL [2]. *In-situ* XAS measurements for the IL/electrode interface were performed at BL3U at UVSOR-III, by using an electrochemical liquid flow cell [1]. The IL was sandwiched with two SiC membranes in the He-filled chamber and XA spectra were measured in transmission mode for the nitrogen, oxygen, and fluorine K-edge regions. The photon energy was calibrated by the first peak in the nitrogen or oxygen K-edge region for a ProLINE polymer thin film in a vacuum chamber [3]. The thickness of the IL film was controlled with the He pressure [4]. The platinum film deposited at the inner surface of one of the two SiC membranes was used as the working electrode. Pt wires, as the quasi-reference and counter electrodes, were located aside the film region inside the electrochemical cell. The potential of the working electrode with respect to the quasi-reference electrode was controlled using a potentiostat.

Figure 1 shows fluorine K-edge XA spectra for the IL/platinum interface at three different potentials. At 0 V (black dashed line), where no IL-ion accumulation/depletion occurs at the interface and therefore the interfacial structure corresponds to the bulk one, double sharp peaks were discernible at the absorption edge around 688 and 692 eV, both of which originate from FSA$^-$, according to a prediction using the GSCF3 code for inner-shell excitation [5]. When negative potentials were applied at the IL/platinum interface, the XA spectra (Fig.1, blue and green lines) showed three potential-dependent features. First, the lowest-energy peak decreased in intensity and blue-shifted. Second, the second lowest-energy peak was broadened. Third, the intensity at the high-energy region became higher. These three features demonstrate that the present XAS measurements in transmission mode with a nm-scale thin film setup sensitively detect the interfacial structure, which is different from the bulk one and is also potential-dependent. Oxygen and nitrogen K-edge XA spectra (data not shown) exhibited similar potential-dependent features, although the behavior for the lowest-energy peak was element-dependent. Furthermore, the oxygen K-edge spectra at negative potentials showed an evolution of pre-edge peak, which clearly indicates the formation of solid electrolyte interphase (SEI). SEI, which is indispensable for a stable battery anode and therefore has been extensively studied, is generally difficult to investigate in an *in-situ* manner, illustrating the powerfulness of the present *in-situ* XAS method. The SEI formation is highly likely to cause the intensity increases at the high-energy region observed for all three elements, as exemplified in Fig.1 for the fluorine case.

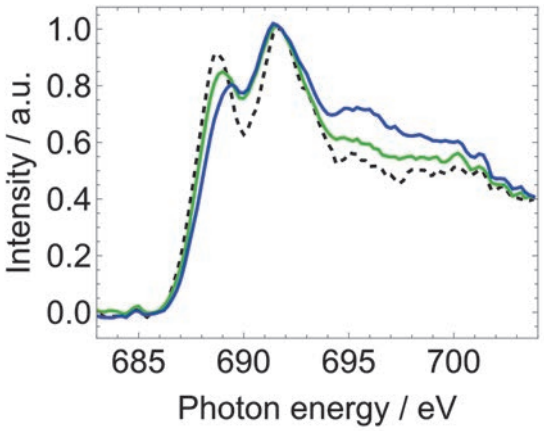

Fig. 1. Fluorine K-edge XA spectra for the IL/platinum interface at 0 (black dashed), −2 (green), and −2.5 V (blue).

[1] M. Nagasaka *et al.*, Rev. Sci. Instrum. **85** (2014) 104105.
[2] S. Kato *et al.*, J. Electrochem. Soc. **169** (2022) 076509.
[3] M. Nagasaka *et al.*, J. Electron Spectrosc. Relat. Phenom. **224** (2018) 93.
[4] M. Nagasaka *et al.*, J. Electron Spectrosc. Relat. Phenom. **117** (2010) 130.
[5] N. Kosugi, Theor. Chim. Acta **72** (1987) 149.

BL3U

Cation-Specific Effects on Interfacial Water Structure Around Silica Nanoparticles Probed by O K-edge NEXAFS

X.Kong[1], N. Faure[1], M. Nagasaka[2] and Z. Abbas[1]

[1]*Department of Chemistry and Molecular Biology, Atmospheric Science, University of Gothenburg, SE-413 90 Gothenburg, Sweden*

[2]*UVSOR Synchrotron, Institute for Molecular Science, Okazaki 444-8585, Japan*

Understanding the interfacial water structure at the nanoparticle-electrolyte interface is essential for advancing applications in catalysis, separation science, environmental remediation, and biomedicine. Silica nanoparticles (SiO_2), which develop surface charge through silanol group deprotonation, offer a model system for such studies. The organization of water around these charged particles—strongly influenced by particle size, shape, concentration, and particularly the type of counterion, remains poorly resolved, especially at the nanoscale [1].

In this beamtime at the BL3U beamline (UVSOR-III), we investigated cation-specific effects on interfacial water structures in colloidal dispersions of silica nanoparticles using oxygen K-edge Near Edge X-ray Absorption Fine Structure (NEXAFS) spectroscopy. In this preliminary study, nanoparticles (8-10 nm) were suspended in aqueous media with Na^+ as the stabilizing counterion at various concentrations (10-30 wt%). The experiment builds on recent studies showing interfacial water perturbations induced by nanodiamond surfaces [2] and is a precursor to planned systematic studies involving a full alkali series (Li^+, Na^+, K^+, Rb^+, Cs^+).

Measurements were performed in a liquid flow cell configuration, where liquid samples were sandwiched between two 100 nm thick Si_3N_4 membranes (window area: 2 × 2 mm²) with 100 µm Teflon spacers. Liquid exchange was achieved in situ via tubing pump, with temperature controlled at ~25°C. A 200 × 200 µm² beam spot was selected to optimize photon flux.

Oxygen K-edge NEXAFS spectra were collected and analyzed to investigate the characteristic spectral features corresponding to different water environments: the pre-edge (~535 eV), main-edge (~537 eV), and post-edge (~540 eV), as shown in Fig. 1. These features provide insight into the electronic structure and hydrogen bonding states of water molecules near nanoparticle surfaces. To correct for potential variations in liquid film thickness and to enable direct comparison across different conditions, the spectra were normalized either to the intensity at the pre-edge or post-edge region.

In this study, the SiO_2 nanoparticle concentration was fixed at 15 wt%, and the key variable was the type of dissolved cation—Li^+, Na^+, K^+, Cs^+, NH_4^+, as well as multivalent anion-containing salts like Na_2SO_4 and K_2SO_4. Despite the constant nanoparticle loading, the post-edge intensities exhibited noticeable variation depending on the cation present. In general, larger or less strongly hydrated cations (e.g., Cs^+, NH_4^+) led to enhanced post-edge features, which suggests a more ordered or polarized water structure at the nanoparticle interface. This may be attributed to differences in ion hydration behavior and their impact on the arrangement of water molecules in the electrical double layer.

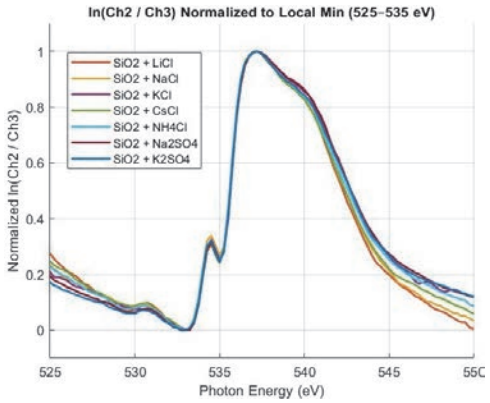

Fig. 1. O K-edge NEXAFS spectra of 15 wt% SiO_2 nanoparticle solutions in the presence of different salts: LiCl, NaCl, KCl, CsCl, NH_4Cl, Na_2SO_4, and K_2SO_4. All measurements were conducted at 25 °C. The spectra have been normalized both to the post-edge maximum and the pre-edge feature to account for differences in sample thickness and to facilitate comparison of spectral features across different ionic conditions.

Conversely, the pre-edge intensity—which reflects contributions from distorted or weakly hydrogen-bonded water species—was found to decrease for certain salts, indicating that specific cations can promote stronger hydrogen bonding or more structured water layers near the surface. These ion-specific trends point to the subtle yet significant influence of cation size, charge density, and hydration enthalpy on interfacial water structuring.

These results are consistent with prior molecular dynamics simulations and spectroscopic studies showing that cation identity modulates interfacial water orientation and hydrogen bonding patterns. The findings reinforce the capability of soft X-ray absorption spectroscopy to sensitively detect changes in interfacial solvent structure induced by ion-specific interactions, even in complex colloidal systems.

[1] Abbas *et al.*, J. Phys. Chem. C **112** (2008) 5715.
[2] T. Petit *et al.*, J. Phys. Chem. Lett. **6** (2015) 2909.

III-4

BL3B

Evaluation of Properties of Inner Region of Zinc Aluminate Thin Film for Ultra violet Emission

H. Kominami[1,2,3], J. Kamikawa[1], T. Sadamori[1], D. Takeya[1], M. Yasuda[1], N. Yoshimura[1], K. Kamiya[2], H. Nagao[2], K. Murata[2], K. Yamaguchi[2] and S. Kurosawa[4,5]

[1]*Graduate School of Integrated Science and Technology, Shizuoka University,*
[2]*Faculty of Engineering, Shizuoka University,*
[3]*Graduate School of Science and Technology, Shizuoka University,*
[1~3]*3-5-1 Johoku, Chuo-ku, Hamamatsu 432-8651 Japan*
[4]*New Industry Creation Hatchery Center (NICHe), Tohoku University 6-6-10 Aza-Aoba, Aramaki, Aoba-ku, Sendai, Miyagi 980-8579, Japan*
[5]*Faculty of science, Yamagata University, 1-4-12, Kojirakawa-machi, Yamagata 990-8560, Japan*

In the fields of sterilization and water purification, conventional sterilization methods using chemicals and heat are concerned about the effects of deterioration, toxicity to the human body, and the effects of resistant bacteria. For this reason, sterilization methods using ultraviolet light are becoming more widespread. It is said that ultraviolet light around 260 nm has the strongest effect. Mercury lamps and other devices are used as ultraviolet light sources for sterilization, but their use is concerned from the perspective of environmental impact. Under these circumstances, we aim to develop a new ultraviolet light-emitting device for sterilization that is highly efficient, low-cost, and has a low environmental impact. As one of these devices, we focused on a device that uses $ZnAl_2O_4$, which emits deep ultraviolet light around 250 nm when excited by electron beams, as the emitting layer. We are currently working on the fabrication of a double-insulated electroluminescence (EL) lamp, which is one of the solid-state display elements. There are many challenges in developing this device, such as improving the sterilization ability, controlling the voltage applied to the emitting layer, and fabricating an ultraviolet-transparent electrode. In particular, it is necessary to know the dielectric constant of the emitting layer to control the applied voltage, but the dielectric constant of the emitting layer $ZnAl_2O_4$ is currently unknown. Therefore, we attempted to obtain the refractive index from the fluctuation of the transmittance spectrum of the emitting layer, and from that, to obtain the dielectric constant.

On a c-plane sapphire substrate (c-Al_2O_3), he deposited about 300 nm of ZnO by magnetron sputtering, and on top of that he deposited about 25 nm of Al_2O_3 as a cap layer. After sputtering, he fabricated $ZnAl_2O_4$ thin films by annealing (990°C, 50 hours) under atmospheric conditions in a muffle furnace and by thermal diffusion. In addition, the thin film surface of the prepared sample was etched using hydrochloric acid to expose the inside of the film, and its characteristics were evaluated using cathodo-luminescence (CL), thin film X-ray diffraction measurement (XRD), analytical FE-SEM, and transmission.

The transmission spectrum of the sample etched for 0 to 300 minutes (0 to 450 nm) is shown in Fig. 1. Interference was observed at wavelengths of 180 to 350 nm. Here, the wavelengths of the peaks of the spectrum fluctuation are λ1, λ3, and λ5 from the short wavelength side, and the wavelengths of the valleys are λ2 and λ4, and we tried to derive the refractive index from these wavelengths.

From the cathodoluminescence measurement, the emitting layer region is calculated to be about 1200 nm. Therefore, calculations were performed assuming that Zn diffusion is 1000 and 1400 nm. As a result, when the diffusion length is assumed to be 1000 nm, the refractive index is about 4 to 5. On the other hand, when the diffusion length is assumed to be 1400 nm, the refractive index is about 3. From past research, it is thought that a layer of Zn diffused into the sapphire substrate is formed inside the thin film. In addition, the dielectric constant of the sapphire substrate is 9, and the refractive index is converted to about 3 without considering the extinction coefficient. From these facts, it is considered appropriate to assume that the refractive index after 450 nm etching is about 3, and that the Zn diffusion length is 1400 nm. In addition, because a good $ZnAl_2O_4$ layer is formed from the surface to about 400 nm, the refractive index is thought to be about 1.9 to 2.3, and the dielectric constant is thought to be about 3.6 to 5.3.

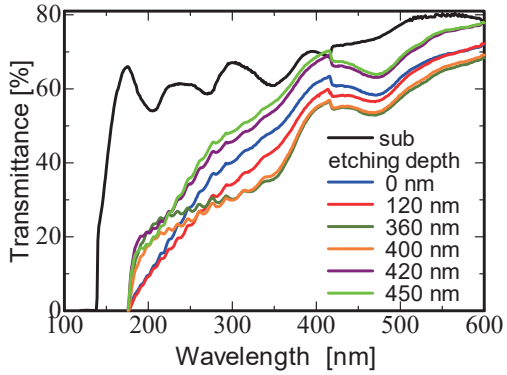

Fig. 1. Transmission spectra of etched $ZnAl_2O_4$ thin films.

BL4U

Scanning Transmission X-ray Microscopy (STXM) Study of Co Oxidation State Evolution in Nano- and Micro-Sized $LiCoO_2$ During Alkaline OER

Y. Zhang[1], J. Lei[1], T. Araki[2] and J. Wang[1]
[1]*City University of Hong Kong, Kowlong, Hong Kong*
[2]*UVSOR Synchrotron Facility, Institute for Molecular Science, Okazaki 444-8585, Japan*

Layered $LiCoO_2$ (LCO), well-known as a cathode in lithium-ion batteries, also shows promise as an alkaline oxygen evolution reaction (OER) electrocatalyst due to its $Co^{3+}\leftrightarrow Co^{4+}$ redox activity and robust Co–O framework [1]. Studies have demonstrated that Na^+ or K^+ incorporation in LCO can enhance Co–O covalency, boosting OER activity while preserving structural integrity [2]. Nanoscale LCO, in particular, offers abundant Co^{3+}-rich surface facets and favorable electronic structures for redox kinetics. Conversely, micro-sized LCO (mLCO) often suffers from limited lithium diffusion, surface Co dissolution, and structural reconstruction under prolonged OER conditions [3,4].

To explore how particle size influences Co valence state distribution during OER, we performed STXM with Co L_3-edge XANES on nanoparticulate LCO (nLCO, ≈ 50 nm) and micron-sized LCO (mLCO, ≈ 1 μm). Samples were polarized in 1 M KOH at 1.5 V vs. RHE for 10 min and 30 min. We aimed to determine: (i) initial oxidation homogeneity, (ii) short-term oxidation evolution, and (iii) spatial heterogeneity after prolonged exposure.

STXM maps of pristine samples showed that nLCO consistently exhibited an XANES peak at 778.0 eV, indicating a homogeneous Co^{3+} oxidation state (Fig. 1a). In contrast, mLCO displayed a broader peak around 776.8 eV, signifying mixed Co^{2+}/Co^{3+} states and a lower overall oxidation level (Fig. 1b). The enhanced surface energy and electronic coupling in nLCO likely stabilize Co^{3+}, consistent with previous findings on size-dependent structural robustness [1, 3].

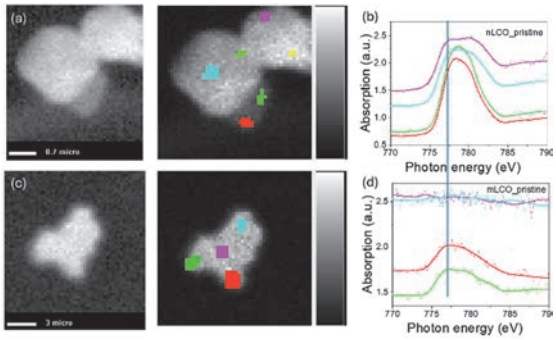

Fig. 1. STXM of nLCO pristine (a-b) and mLCO pristine (c-d).

After 10 minutes of OER polarization, the Co peak in nLCO slightly shifted to ~777.8 eV but remained indicative of Co^{3+} (Fig. 2a). Remarkably, mLCO's peak shifted from 776.8 to ~777.9 eV (Fig. 2b), aligning with nLCO. This reveals rapid oxidation of surface Co^{2+} to Co^{3+} in mLCO, demonstrating that even micro-sized particles can achieve surface valence homogenization under short-term OER conditions.

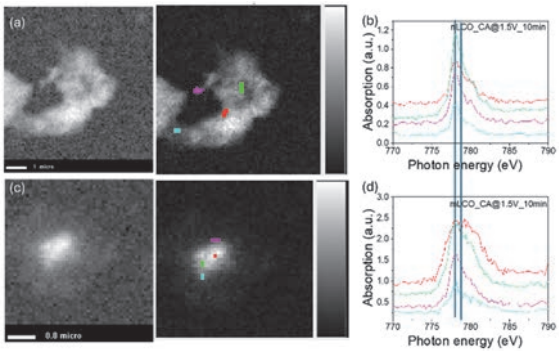

Fig. 2. STXM of nLCO (a-b) and mLCO (c-d) after CA at 1.5V for 10min.

Prolonged polarization showed divergent trends: nLCO retained uniform Co^{3+} distribution with no spatial variation (Fig. 3a) while mLCO developed clear spatial heterogeneity—edge regions exhibited peaks at ~778.0 eV (possibly over-oxidized Co^{3+}), while core areas remained around ~777.8 eV (Fig. 3b). This behavior results from rapid edge oxidation by OH^- and slower lithium deintercalation in the core, leading to non-uniform internal oxidation—a phenomenon observed in larger LCO crystals [4].

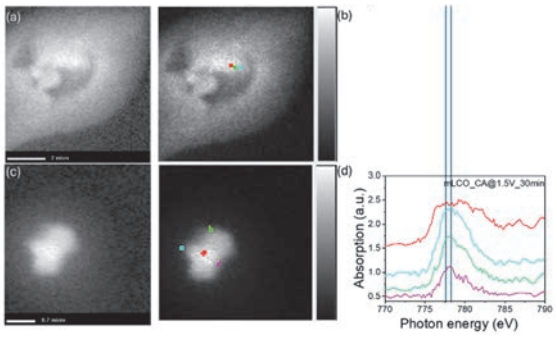

Fig. 3. STXM of nLCO (a-b) and mLCO (c-d) after CA at 1.5V for 30min.

[1] Y. Kim *et al.*, J. Mater. Chem. A **10** (2022) 10967.
[2] J. Qian *et al.*, Nat. Commun. **9** (2018) 4918.
[3] Y. Kim *et al.*, J. Phys. Chem. Lett. **6** (2015) 1357.
[4] T. Maiyalagan *et al.*, Nat. Commun. **6** (2015) 3949.

BL4U

In Situ STXM-Based Approach to Visualize Polymer Fracture: Demonstration with Polystyrene

T. Ejima[1,2], E. Sasaki[2] and Y. Tamura[3]
[1]*SRIS &* [2]*IMRAM, Tohoku University, Sendai 980-8577, Japan*
[3]*ENEOS Materials Corp., Yokkaichi 510-0871, Japan*

Polystyrene (PS) is a widely used thermoplastic owing to its low cost, high transparency, and ease of processing. The fracture behavior of PS is primarily attributed to main-chain scission, in which carbon–carbon bonds within the polymer backbone are ruptured—a phenomenon widely observed in polymeric systems. Although molecular probes such as fluorescent dyes and stabilized radicals have facilitated the visualization of such events, methods for directly detecting main-chain scission remain limited [1].

Carbon K-edge spectral imaging at sub-micron resolution is expected to reveal stress-induced electronic structural changes and elucidate fracture mechanisms, with a particular focus on main-chain scission [2]. The objective of this study is to visualize polymer fracture without the use of dyes or radicals by performing in situ stress-application experiments using scanning transmission X-ray microscopy (STXM). To this end, a custom-designed sample holder was developed by integrating the STXM frame from BL4U (UVSOR) with a cartridge designed for simultaneous tensile deformation and TEM observation [3]. The holder incorporates a piezo-linear actuator (Picomotor™, Model 8302, Newport) connected to a lever, enabling precise displacement control (Fig. 1a). The cartridge contains a flexure structure that is actuated by the lever, thereby applying stress to the sample (Fig. 1b). Polymer samples were mounted on parallel TEM grids and secured with double-sided adhesive tape. The conversion of vertical lever motion into horizontal displacement resulted in an opening displacement of 9.02 ± 0.18 nm per actuator pulse.

The measurements were conducted using injection-grade polystyrene (HF77, PS Japan Corporation), which was sectioned into 100 nm-thick slices using an ultramicrotome. These slices were mounted on TEM grids (40 μm bar width, 62 μm pitch) and affixed to the cartridge. During STXM, soft X-rays from the BL4U monochromator were focused to a 50 nm spot using a zone plate. The images were acquired with a pixel exposure time of 2 ms.

Two stress-application measurements were conducted, both showing PS fracture at strain levels between 0.327 and 0.460. Below 0.327, the STXM spectra from the PS region exhibited consistent profiles (Fig. 2) corresponding to previously reported PS spectra [2]. Normalized absorption spectra revealed a strain-dependent increase near 285 eV (inset of Fig. 2), consistent with π* orbitals from benzene rings [2, 4], indicating alignment of the ring along the X-ray direction [4]. These results suggest that stress-application STXM offers enhanced potential for elucidating polymer fracture mechanisms.

Acknowledgement:
The authors thank the Machine Shop of IMRAM, Tohoku University for their support in fabricating the STXM holder.

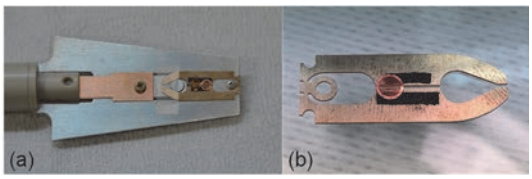

Fig. 1. (a) STXM holder frame with a piezo-linear actuator, (b) Sample cartridge: Stress is applied to the sample by opening and closing the flexure structure.

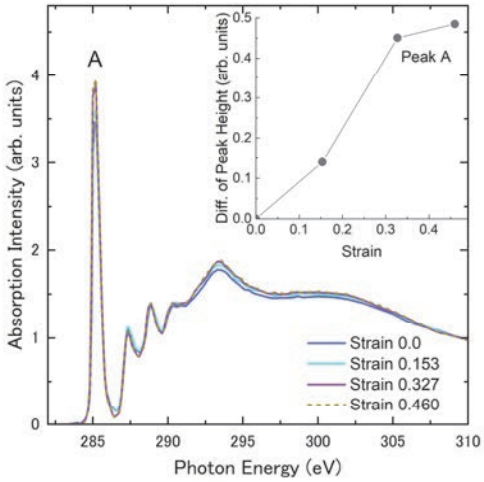

Fig. 2. Spectral shape the major area is the same of PS [2]. Inset is the intensity change of peak A.

[1] T. Yamamoto, D. Aoki and H. Otsuka, ACS Macro Lett. **10** (2021) 744.
[2] J. Stöhr, *NEXAFS Spectroscopy* (Springer, Berlin & Heidelberg, 1992) §7.4, p.230.
[3] T. Higuchi *et al*., Microscopy **67** (2018) 296.
[4] J. A. Horsley *et al*, J. Chem. Phys., **83**(12) (1985) 6099.

BL4B

Coverage-Dependent Spin Reorientation Transition in Ni Thin Films on Cu(001) Induced by Pd Overlayers

T. Miyamachi[1,2], N. Okamura[1], A. Iwai[1], H. Ono[1], N. Maejima[3,4], O. Ishiyama[3,4], E. Nakamura[5], H. Iwayama[5], T. Yokoyama[3,4] and M. Mizuguchi[1,2]

[1]*Department of Materials Science and Engineering, Nagoya University, Nagoya 464-8603, Japan.*
[2]*Institute of Materials and Systems for Sustainability (IMaSS), Nagoya University, Nagoya 464-8601, Japan.*
[3]*Institute for Molecular Science, Myodaiji-cho, Okazaki 444-8585, Japan*
[4]*The Graduate University for Advanced Studies, Myodaiji-cho, Okazaki 444-8585, Japan*
[5]*UVSOR Synchrotron Facility, Institute for Molecular Science, Okazaki 444-8585, Japan*

Thin film heterostructures have been widely studied because of novel phenomena developed by the formation of the heterointerface. Especially for the heterostructure composed of magnetic materials, interface conditions such as lattice strain, mixing drastically change magnetic properties of the whole system [1]. In this study, we fabricate Pd/Ni thin film heterostructures on Cu(001) and investigate their structural, electronic, and magnetic properties by low energy electron diffraction (LEED) and x-ray absorption spectroscopy/magnetic circular dichroism (XAS/XMCD). Ni thin films grown on Cu(001) are known to exhibit the spin reorientation transition (SRT) from in-plane magnetization to out-of-plane magnetization with increasing the coverage [2]. Since the SRT is associated with changes in the lattice constant near surface, adding Pd overlayers with significantly larger lattice constant than Ni can modify magnetic properties of Ni thin films by the formation of Pd/Ni heterointerface.

To fabricate Pd/Ni thin film heterostructures, we grow 6 and 12 monolayer (ML) Ni thin films on Cu(001) at room temperature. Then, 2, 6 and 12 MLs of Pd overlayers are grown onto each Ni thin film. LEED patterns of Pd/Ni thin-film heterostructures reveal that both Ni and Pd layers grow epitaxially on Cu(001) but the surface lattice constant of Ni expands by adding Pd overlayers. To investigate electronic, and magnetic properties of Pd/Ni thin film heterostructures, XAS/XMCD measurements are performed at BL4B in UVSOR by total electron yield mode at B = 0 - ± 5 T and T = 6.6 K. The XMCD spectra are obtained at the normal (NI: θ = 0°) and the grazing (GI: θ = 55°) geometries by detecting $\mu_+ - \mu_-$, where μ_+ (μ_-) denotes the XAS recorded at Ni and Pd L adsorption edges with the photon helicity parallel (antiparallel) to the sample magnetization. Note that θ is the angle between the sample normal and the incident x-ray. Element specific magnetization curves of Ni layers are also recorded by plotting the Ni XAS L_3 peak intensity normalized by L_2 one as a function of the magnetic field. The deposition rates and coverages of Ni and Pd layers are crosschecked by the quartz-crystal microbalance (QCM) and XAS edge jumps at L-edges of Ni and Pd relative to of Cu L-edge [3].

We first investigate magnetic properties of bare Ni thin films on Cu(001) by XAS/XMCD. Comparing XAS/XMCD spectra recorded in the NI and GI geometries, we reveal that 6 ML Ni thin films show strong in-plane magnetization the easy magnetization direction of 12 ML Ni thins film is slightly toward the out-of-plane direction, which is in good agreement with previous work investigated by ferromagnetic resonance measurements [2].We find from Pd coverage dependence of Ni magnetization curve that adding Pd overlayer modifies the magnetic anisotropy of Ni thin films. For 12 ML Ni thin films, the easy magnetization direction gradually shifts from out-of-plane to in-plane direction with increasing Pd coverage. On the other hand, adding Pd overlayer further stabilizes the in-plane magnetization of 6 ML Ni films. Interestingly, the stabilization of the in-plane magnetization is completed when 2 MLs of Pd are deposited no further changes are recognizable with increasing Pd coverage. The results indicate that the degree of lattice strain of Ni induced by Pd overlayers and the hybridization strength at the Pd/Ni heterointerface, which both modify the magnetic anisotropy of Ni thin film, are strongly dependent on Ni coverage.

[1] S. Nakashima *et al*., Adv. Funct. Mater. **29** (2019) 1804594.
[2] B. Schulz *et al*., Phys. Rev. B **50** (1994) 13467.
[3] H. Ono *et al*., J. Phys. Chem. C **127** (2023) 23935.

BL4B

Spin Reorientation Transition of Co Nano Islands by the Formation of Organic-Inorganic Hybrid Interface

T. Miyamachi[1,2], H. Ono[1], K. Fujimoto[1], K. Yoshida[1], N. Maejima[3,4], O. Ishiyama[3,4], E. Nakamura[5], H. Iwayama[5], T. Yokoyama[3,4] and M. Mizuguchi[1,2]

[1]*Department of Materials Science and Engineering, Nagoya University, Nagoya 464-8603, Japan.*
[2]*Institute of Materials and Systems for Sustainability (IMaSS), Nagoya University, Nagoya 464-8601, Japan.*
[3]*Institute for Molecular Science, Myodaiji-cho, Okazaki 444-8585, Japan*
[4]*The Graduate University for Advanced Studies, Myodaiji-cho, Okazaki 444-8585, Japan*
[5]*UVSOR Synchrotron Facility, Institute for Molecular Science, Okazaki 444-8585, Japan*

An organic-inorganic hybrid interface has attracted attention due to its controllable interface electronic state by the proper choice of organic and inorganic materials. Especially for the system composed of organic molecules and an inorganic magnetic material, a variety of novel spin functionalities with the help of long spin diffusion length of organic molecule can emerge via the magnetic interaction at the organic-inorganic interface. Since the degree of the magnetic interaction strongly replies on the spin polarization of the inorganic magnetic material near the Fermi energy, element specific investigations of the organic-inorganic hybrid interface are important to understand the impact of the formation of the organic-inorganic hybrid interface on the magnetic properties of the inorganic magnetic material. In this work, we fabricate the organic-inorganic hybrid interface composed of [1,2,5] Thiadiazolo [3,4-f][1,10]phenanthroline 1,1-dioxide ($tdapO_2$) and Co nano island and investigate its electronic/magnetic properties element specifically by x-ray absorption spectroscopy/x-ray magnetic circular dichroism (XAS/XMCD).

XAS/XMCD measurements are conducted at BL4B in UVSOR by total electron yield mode at B = 0 - ± 5 T and T = 7.7 K. The XMCD spectra are obtained at the normal (NI: θ = 0°) and the grazing (GI: θ = 55°) geometries by detecting $\mu_+ - \mu_-$, where μ_+ (μ_-) denotes the XAS recorded at Co L adsorption edges with the photon helicity parallel (antiparallel) to the sample magnetization. Note that θ is the angle between the sample normal and the incident x-ray. Magnetization curves of Co nano islands are recorded by plotting the L_3/L_2 Co XAS peak intensity as a function of the magnetic field.

Co islands are first grown by deposition of 0.4 monolayer Co onto Cu(111) at room temperature. We investigate the morphology of Co islands by scanning tunneling microscopy (STM) in advance, and confirm the formation of isolated bilayer Co nano islands at Co coverage of 0.4 monolayer. The deposition rate of Co is evaluated by the quartz-crystal microbalance (QCM) and XAS edge jump [1]. Then, $tdapO_2$ molecules are sublimated by heating at 380 K and deposited onto Co islands. The deposition amount of $tdapO_2$ is evaluated by QCM and set to several molecular layers in this study.

In XAS/XMCD measurements, we focus on the remanent magnetization and coercivity in the Co magnetization curve. While the Co magnetization curve recorded in the GI geometry shows a clear hysteresis loop, reduced remanent magnetization and a smaller hysteresis loop are observed for that recorded in the NI geometry. The results reveal in-plane magnetic easy axis of Co nano islands, which is consistent with previous study [2]. After the deposition of $tdapO_2$, significant changes are observed for Co magnetization curve recorded in the NI geometry. We find that the remanent magnetization increases by a factor of two, and the coercivity by a factor of seven, which induces the spin reorientation transition (SRT) of Co nano islands from in-plane direction to out-of-plane direction. These results indicate that substantial enhancement of perpendicular magnetic anisotropy of Co nano island is caused by the interface formation with $tdapO_2$. In future work, we will investigate the adsorption geometry and electronic structures of $tdapO_2$ molecules by STM and discuss the origin of the SRT of Co nano islands.

[1] H. Ono *et al*., J. Phys. Chem. C **127** (2023) 23935.
[2] M. Zhang *et al*., J. Phys.: Condens. Matter **12** (2000) 783.

Angle-Resolved Photoemission Circular Dichroism for Chiral Molecule Overlayer on Monolayer WS_2

F. Nishino[1,2], K. Fukutani[1,2], P. I. Jaseela[1,2], J. Brandhoff[3], F. Otto[3], M. Grünewald[3], M. Schaal[3], J. Picker[4], Z. Zhang[5], A. Turchanin[4], S. Makita[6], H. Iwayama[6], T. Hirose[5], T. Fritz[3] and S. Kera[1,2,6]

[1]*Institute for Molecular Science, Okazaki 444-8585, Japan*
[2]*School of Physical Sciences, The Graduate University for Advanced Studies, Okazaki 444-8585, Japan*
[3]*Institute of Solid State Physics, Friedrich Schiller University Jena, Helmholtzweg 5, 07743 Jena, Germany*
[4]*Institute of Physical Chemistry, Friedrich Schiller University Jena, Lessingstraße 10, 07743 Jena, Germany*
[5]*Institute for Chemical Research, Kyoto University, Gokasho, Uji, Kyoto 611-0011, Japan*
[6]*UVSOR Synchrotron Facility, Institute for Molecular Science, Okazaki 444-8585, Japan*

A chirality-induced spin selectivity (CISS) effect with controlled chiral molecules on various solid surfaces has been actively studied for various applications, such as for spintronics and enantio-separations [1]. On the other hand, many aspects of this phenomenon, including its mechanism underlying its extraordinarily large spin polarization effects, remain unknown.

Our approach to this challenge is to fabricate well-defined chiral molecular systems on solid surfaces with known spin-polarized electronic band structures, and to investigate how the surface chirality affects the emitted electrons from the solid by angle-resolved photoemission spectroscopy (ARPES).

As a preliminary study, in this work, we used angle-resolved photoemission circular dichroism (CD-ARPES) for the system of chiral molecular overlayer on achiral substrate possessing fully spin-polarized electrons to assess how the electrons emitted from the substrate recognize the surface chirality.

The enantiopure chiral molecule, thiadiazole-[9] helicene (TD[9]H) [2], was used in this study as show in Fig. 1(a). The substrate used was a monolayer WS_2/Au(111) (ML-WS_2) with fully spin-polarized bands at $\overline{K}$' and $\overline{K}$ points [3]. After depositing the enantiopure TD[9]H on the ML-WS_2 under ultra-high vacuum condition, low-energy electron diffraction (LEED) showed an ordered molecular overlayer with broken mirror-symmetry, indicating the surface chirality has been induced on the system.

Following the confirmation of the surface chirality, CD-ARPES measurements were performed, using left circularly polarized (LCP) and right circularly polarized (RCP) lights for both the clean substrate and the (*M*)-TD[9]H/ML-WS_2 samples, as shown in Fig. 1(b).

Figures 1(c)-(e) show the CD-ARPES maps obtained for clean ML-WS_2 substrate. It can be seen that the dichroic signals at the $\overline{\Gamma}$-$\overline{M}$ plane [black dotted lines in Figs. 1(c), 1(d) and the entire map in Fig. 1(e)], which is the mirror plane of the substrate, is very weak. Furthermore, the dichroic signals in the $\overline{\Gamma}$-$\overline{K}$ and $\overline{\Gamma}$-$\overline{K}$' directions are seen to be generally anti-symmetric with respect to the $\overline{\Gamma}$-$\overline{M}$ plane.

These characteristics of dichroic signals from

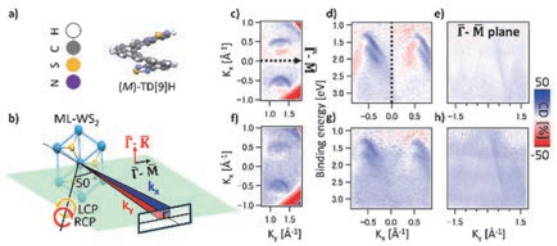

Fig. 1. (a) Molecular structures of (*M*)-TD[9]H. (b) Schematic illustration of CD-ARPES setup. The relative orientations of the sample and the photoelectron analyzer slit are shown. (c)-(e) CD-ARPES map of ML-WS_2. (f)-(h) CD-ARPES map of (*M*)-TD[9]H/ML-WS_2. (c) and (f) shows constant-energy cut and (d), (g) is the intensity plots in E-k_x slice. (e) and (h) is the intensity plots in E-k_y slice.

substrate can readily be understood from the point of view of symmetry. Since the substrate is achiral and the mirror plane of the crystal coincides with the plane of light incidence, it must hold that $I_{RCP}(k_x, k_y) = I_{LCP}(-k_x, k_y)$ (Equation 1), where I_{RCP} and I_{LCP} are the photoelectron intensities with RCP and LCP lights, respectively. That is, the achirality of substrate is reflected in our CD-ARPES results.

Next, the CD-ARPES results after the deposition of (*M*)-TD[9]H are shown in Figs. 1(f)-(h). Unlike the CD-ARPES results from the clean substrate, finite (blue) dichroic signals were observed uniformly in the substrate bands, molecular orbitals and inelastic scattering regions even in the E-k slice of the $\overline{\Gamma}$-$\overline{M}$ plane as can be seen in Fig. 1(h). While more investigations are necessary, the apparent violation of equation 1 above could arise from the loss of achirality (i.e., emergence of chirality) for the electrons in the system of chiral molecular overlayer on achiral substrate.

[1] S.-H. Yang *et al*., Nat. Rev. Phys. **3** (2021) 328.
[2] Z. Zhang *et al*., Tetrahedron **142** (2023) 133514.
[3] P. Eickholt *et al*., Phys. Rev. Lett. **121** (2018) 136402.

BL5U

Growth of P Ultra-Thin Film on Cu(111)

N. Maejima[1] and T. Yokoyama[1]
[1]*Institute for Molecular Science, Myodaiji-cho, Okazaki 444-8585, Japan*

Two-dimensional single-element materials, such as graphene, silicene and germanene etc., have attracted much attention owing to their unique physical and chemical properties. Phosphorene, has attracted attention due to its high mobility and variable band gap depending on the number of atomic layers. Blue phosphorene with a Dirac cone, produced by evaporation of P on a heated Cu(111) substrate, was recently reported [1]. The 1 ML and 1.5 ML blue phosphorene samples show 10√3x 10√3 and 13 x 13 moire LEED patterns, respectively. The formation of self-assembled P nanodots on top of the phosphorene sheet of 13x13 sample was clearly observed in the study. In this report,1ML phosphorene was grown on Cu(111) which shows 13x13 moire LEED pattern in different fabrication process.

Experiments were performed at BL5U of the UVSOR facility. The Cu(111) surface was cleaned by cycles of Ar^+ ion spattering (0.75 keV) and annealing (600 °C). P atoms were deposited by directly heating of a piece of GaP wafer. The Cu(111) substrate was kept at 300 °C during the P atoms deposition. The prepared Cu(111) and P deposited Cu(111) samples showed 1x1 and 13x13 moire LEED patterns, respectively. The P deposited sample were post-annealed at 500°C. The LEED pattern was not changed from of this sample consisted of 1x1 spots arising from 13x13 moire LEED pattern. P 2p and valence band photoelectron spectroscopy (PES) measurements were performed by an MBS A-1 analyzer.

Figure 1 shows the P 2p spectrum obtained from P deposited during 300°C annealing and 500°C post-annealing samples with black and red solid lines, respectively. In the spectrum of the P deposited sample during 300°C annealing, P 2p 3/2 peak of shoulder and main components were observed at 128.3 eV and 128.8 eV, respectively. These peak components were attributed to the P nanodot and blue phosphorene layer, respectively, in the previous study [1]. The 500°C post-annealing sample have only the main component at 128.8 eV. The total area of the P 2p spectrum was reduced to 80% by 500°C post- annealing process. The P nanodot component observed in the spectra of 300°C annealing sample has disappeared, indicating that the whole surface is simply covered with blue phosphorene monolayer. The band dispersion of the valence band of the sample post-annealed at 500 °C showed a linear band around the Cu(111) $\overline{K}$ point. This result is similar to the band structure of 10√3x10√3 1ML Blue Phosphorene sample structure previously reported. Combining these results and the fact that the LEED pattern was not changed by the 500 °C post-annealing process indicates that the 13x13 structure is not due to nanodot origin but to a blue phosphorene monolayer. There are several lattice constants for phosphorene reported ranging from 3.4 Å to 4.2 Å [1]-[3]. Such flexible lattice constants are attributed to differences in the planarity of the phosphorene layers and surface super structure.

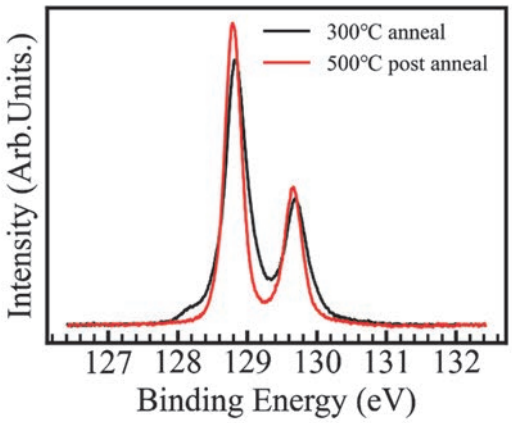

Fig. 1. Figure 1 shows the P 2p spectrum of P deposited during 300°C annealing (black solid line) and 500°C post- annealing samples (red solid line).

[1] Y. Kaddar *et al., Adv. Funct. Mater.* **33** (2023) 2213664.
[2] YH. Song, *et al.,* Nat Commun. **15** (2024) 1157.
[3] D. Zhou, *et al.,* ACS Nano **14** (2020) 2385.

Spin-Resolved Electronic Structure of Altermagnet MnTe and CrSb

M. Zeng[1] and C. Liu[1]
[1]*Southern University of Science and Technology (SUSTech), Shenzhen, Guangdong 518055, China*

Magnetic materials play a crucial role in modern technology, and controlling spins in these materials remain a central challenge in spintronics [1–3]. Large spin-splitting has been observed primarily in ferromagnetic materials and system with strong spin-orbit coupling (SOC). However, strong SOC is typically found in heavy elements, which are often toxic and prone to defects, limiting their practical applications.

Recently, researchers have discovered that light-element collinear antiferromagnets could also exhibit properties that are traditionally inherit to ferromagnets [4–9]. In these systems, SOC is negligible, allowing the spin and lattice degree of freedom to be decoupled. This unique property enables e.g. anomalous Hall effect [10-11] and giant spin splitting [12] in antiferromagnetic materials. Specifically, collinear members of spin-split antiferromagnets are termed *altermagnets* due to their alternatively patterned spin polarization.

Among the many proposed altermagnets, MnTe and CrSb have emerged as key candidates due to their simple magnetic structures, high Néel temperatures, and substantial spin splitting. However, direct spectroscopic measurements of their spin textures remain scarce.

To test the predictions of altermagnetism and provide experimental insights for future applications, we performed spin-ARPES (SARPES) measurements on MnTe and CrSb at this beamtime. The results are presented in Fig. 1 and Fig. 2.

For MnTe, traces of faint bulk bands can be observed [Fig. 1(a)]. However, as shown in Fig. 1(b), SARPES measurements reveal a uniform spin-up polarization within the reliable momentum range, contradicting the theoretical expectation of an antisymmetric spin polarization around the Γ point.

For CrSb, a clear holelike band is visible [Fig. 2(a)]. S_z-resolved MDCs were subsequently measured on the bands near the Fermi level, with an energy integration window of E_B = 0 – 0.5 eV. The SARPES result shows exclusively spin-up polarization, again inconsistent with the altermagnetic theory.

To assess potential instrumental artifacts, we measured the spin polarization of polycrystalline gold, which should ideally yield zero spin signal. However, Fig. 3 reveals strong spin polarization on the gold sample, indicating a significant instrumental bias.

Given that the intrinsic spin polarization in altermagnets is inherently weak, this instrumental background likely dominates the spin signal, masking the spin polarization of the materials. This explains why Fig. 1 and Fig. 2 display similar spin polarization patterns despite their different electronic structures.

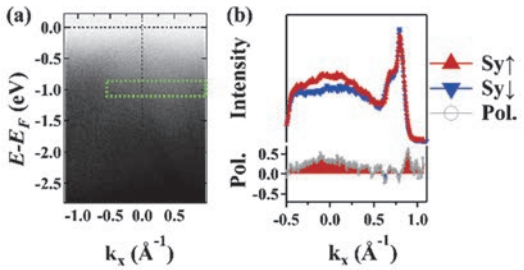

Fig. 1. The SARPES result on MnTe. (a) Spin-integrated ARPES band dispersion acquired at $h\nu$ = 74 eV (k_z = 8.5 π/c). k_x is parallel to $\bar{\Gamma}$–$\bar{M}$.Green dash frame represents the spin-MDC measurement region in (b). (b) Representative S_y-resolved MDC. Red lines with up-triangle / blue lines with down-triangle correspond to SARPES signals for opposite S_y components.

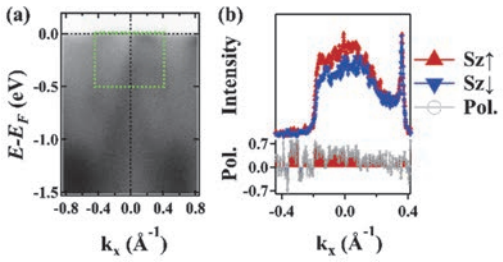

Fig. 2. The SARPES result on CrSb. (a) Spin-integrated ARPES band dispersion acquired at $h\nu$ = 45 eV (k_z = 6.5 π/c). k_x is parallel to $\bar{\Gamma}$–$\bar{M}$. Green dash frame represents the spin-MDC measurement region in (b). (b) Representative S_z-resolved MDC. Red lines with up-triangle / blue lines with down-triangle correspond to SARPES signals for opposite S_z components.

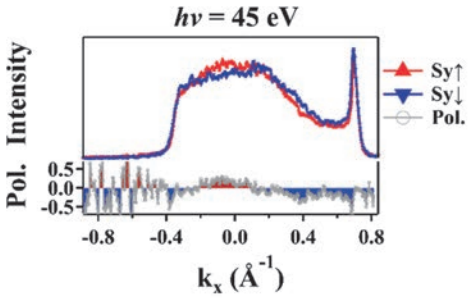

Fig. 3. Representative S_y-resolved MDC on polycrystalline Au at $h\nu$ = 45 eV, E_B = 0.5 eV.

[1] I. Žutić *et al*., Rev. Mod. Phys. **76** (2004) 323.
[2] A. Fert, Thin Solid Films **517** (2008) 2.
[3] C. Chappert *et al*., Nat. Mater. **6** (2007) 813.
[4] L.-D. Yuan *et al*., Phys. Rev. B **102** (2020) 014422.
[5] L.-D. Yuan *et al*., Phys. Rev. Mater. **5** (2021) 014409.
[6] L.-D. Yuan *et al*., Phys. Rev. B **103** (2021) 224410.
[7] S. Hayami *et al*., Phys. Rev. B **101** (2020) 220403.
[8] S. Hayami *et al*., J. Phys. Soc. Jpn. **88** (2019) 123702.
[9] C. Wu *et al*., Phys. Rev. B **75** (2007) 115103.
[10] Z. X. Feng *et al*., Nat. Electron. **5** (2022) 735.
[11] B. R. Gonzalez *et al*., Phys. Rev. Lett. **130** (2023) 036702.
[12] L. Šmejkal *et al*. Phys. Rev. X **12** (2022) 031042.

BL5U, 7U

Interfacial Heavy Fermion in Moiré Kondo Lattice $YbCu_2$/Cu(111)

T. Nakamura[1,2], H. Sugihara[2], Y. Chen[2], K. Nishihara[2], R. Ichikawa[2], H. Yamaguchi[2], K. Tanaka[3] and S. Kimura[1,2,3]

[1]*Graduate School of Frontier Biosciences, The University of Osaka, Suita 565-0871, Japan*
[2]*Department of Physics, Graduate School of Science, The University of Osaka, Toyonaka 560-0043, Japan*
[3]*Institute for Molecular Science, Okazaki 444-8585, Japan*

Heavy fermion (HF) systems originate from a translocation between localized and iterant characters due to the Kondo effect being the host of fertile exotic quantum phases of matter [1]. The Kondo lattice, where rare-earth elements containing localized *f*-electrons are periodically arranged, is the most typical system for investigating HF physics. Recently, HF in stacked layered materials with flat bands near the Fermi level (E_F), such as twisted bilayer graphene and transition metal dichalcogenides, have been actively studied [2-4]. The correlated effect at the interface leads to rich and exotic electronic quantum phases.

Among those correlated stacked systems, the moiré Kondo lattice, a coupled system of two kinds of layered materials by exchange interaction, has been proposed as a new concept in the Kondo lattice model [5-7]. The two layered materials have independent roles for the localized magnetic moment and itinerant conduction electrons. However, the interfacial HF band structure has not been observed experimentally because of poor candidates to satisfy the condition of the moiré Kondo lattice and tiny sample pieces, even in known systems. In this study, we investigated the electronic structure of a novel moiré Kondo lattice $YbCu_2$/Cu(111) by high-resolution synchrotron-based angle-resolved photoemission spectroscopy (ARPES). The $YbCu_2$/Cu(111) is the family of rare-earth-based surface alloy on noble-metal substrates with a moiré superstructure due to the lattice mismatch between the $YbCu_2$ layer with a coherence temperature of 30 K [8] and the Cu(111) substrate.

Figure 1(a) shows the high-resolution ARPES image of $YbCu_2$/Cu(111) near the Fermi level (E_F) taken with linearly polarized 33-eV photons at 15 K. Several hole bands clearly across E_F at around the $\bar{\Gamma}$ point. Note that an asymmetric photoelectron intensity of the Yb^{2+} $4f_{7/2}$ states would be due to a photoexcitation selection rule. In addition to the steep hole band at $k_x = \pm 0.05$ Å^{-1}, which is the upper branch of the 2DHF state on the $YbCu_2$ layer [8], the hole band at $k_x = \pm 0.2$ Å^{-1}, which is folded *sp*-band from Cu(111) substrate [8], was newly observed. Figure 1(b) shows the energy distribution curves of Fig. 1(a) at 0.0 Å^{-1} ($\bar{\Gamma}$ point) and 0.4 Å^{-1} where the peaks originate from the Yb^{2+} $4f_{7/2}$ states. The binding energy at the $\bar{\Gamma}$ point is slightly shifted to the higher by about 10 meV than that at 0.4 Å^{-1}. Such a momentum-dependent energy shift of the Yb^{2+} $4f_{7/2}$ state never appears in the disorder cases, such as single atom adsorption and a randomly diffused Yb atom in a Cu(111) substrate. Furthermore, the left part of the lower branch of the hole band from the Cu(111) substrate smoothly connects to the Yb^{2+} $4f_{7/2}$ flat band, pronouncing band hybridization. These results suggest that a further hybridization between the heavy fermion band of $YbCu_2$ and the bulk *sp*-band derived from Cu(111) substrate is established at the $YbCu_2$/Cu(111) interface.

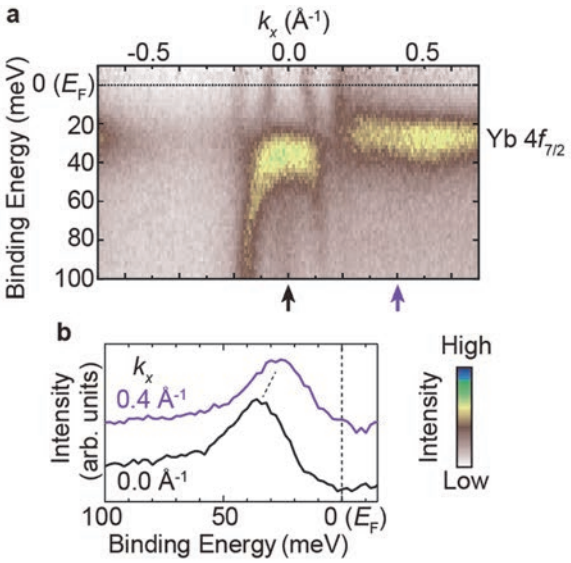

Fig. 1. (a) High-resolution ARPES image near the $\bar{\Gamma}$ point taken with linearly polarized 33-eV photons at 15 K. ARPES intensities are divided by the Fermi–Dirac distribution function convolved with the instrumental resolution. (b) Energy distribution curves at k_x = 0.0 and 0.4 Å^{-1}. The k_x positions are indicated by arrows in (a).

[1] G. R. Stewart, Rev. Mod. Phys. **56** (1984) 755.
[2] Y. Cao *et al*., Nature **556** (2018) 43.
[3] Y. Cao *et al*., Nature **556** (2018) 80.
[4] L. Wang *et al.,* Nat. Mater. **19** (2020) 861.
[5] V. Vaño *et al.,* Nature **599** (2021) 582.
[6] W. Zhao *et al.*, Nature **616** (2023) 61.
[7] W. Zhao *et al.,* Nat. Phys. **20** (2024) 1772.
[8] T. Nakamura *et al.*, Nat. Commun. **14** (2023) 7850.

BL5B

Transmission Spectra of Amorphous Chalcogenide Thin Films in the Vacuum Ultra-Violet Region

K. Hayashi[1]

[1]*Department of Electrical and Electronic and Computer Engineering, Gifu University, Gifu 501-1193, Japan*

Amorphous chalcogenide semiconductor materials, such as amorphous $GeSe_2$, amorphous As_2Se_3 and amorphous Se etc., show a variety of photoinduced phenomena. Therefore, these materials are expected as materials for optoelectronic devices. A lot of work has been done on the photoinduced phenomena of these amorphous semiconductor materials and various mechanisms have been proposed for these photoinduced phenomena [1]. Among those phenomena, the most prominent phenomena are the so-called photodarkening and photobleaching, which are parallel shifts of the optical absorption edge to lower and higher energy sides, respectively, after irradiation with light whose energy corresponds to the optical bandgap. These darkened and bleached states are removed by annealing near the glass-transition temperature. The X-ray diffraction and the volume change of the films before and after irradiation with bandgap light suggest that these phenomena result from the change in the local structure of the amorphous network. However, the details of the mechanisms are still unknown. We are interested in the changes in the optical properties at the higher energy regions. To obtain a wide knowledge of photoinduced phenomena, it is necessary to investigate the photoinduced effects over a wide energy region. In the previous reports, we reported the annealing effect on the VUV transmission spectrum of amorphous selenium [2]. In this report, we focus on the a-$GeSe_2$ thin film that exhibits photobleaching, and report on the investigation of its fundamental optical properties by measuring the VUV transmission spectrum.

Samples used for the measurement of the VUV transmission spectra were thin films of amorphous $GeSe_2$ deposited on a thin aluminum film by conventional evaporation technique. The sample thickness was about 180 nm. An aluminum film of the thickness of 200 nm was used to eliminate the higher order light from the monochromator in the VUV region. These measurements were carried out at room temperature on the BL5B beam line of UVSOR. The spectrum was measured with a silicon photodiode as a detector. Two 1.5mm diameter pinholes were inserted between the monochromator and sample to remove stray light. The intensity of the VUV light was monitored by measuring the TPEY of a gold mesh. The positions of the core levels for the samples were calibrated with reference to the 2p core level absorption of the aluminum film.

Figure 1 shows the VUV transmission spectrum of the amorphous $GeSe_2$ thin film in the wavelength range of 18 to 24 nm. For comparison, the VUV transmission spectra of amorphous As_2Se_3 and amorphous Se are also shown in the figure. As shown in the figure, each spectrum is very broad and multiple shoulders are observed. Main absorption peaks around 22nm correspond to the 3d core level of Se atoms. The absorption spectra observed in amorphous As_2Se_3 and amorphous Se are roughly consistent with the previous report [3]. Although the wavelength resolutions in the spectral measurements are all the same, the spin-orbit splitting of the $3d_{5/2}$ and $3d_{3/2}$ levels of Se atoms is clearly resolved in amorphous $GeSe_2$ and amorphous As_2Se_3, while it is not clearly resolved in as-deposited amorphous Se. The origin of broad spectra and several peaks is not clear. I think that these origins are related to the local structures of the amorphous network. The detailed experiments and analysis will be done in the next step. More detailed experiments are necessary to clarify the origin of the VUV transmission spectra.

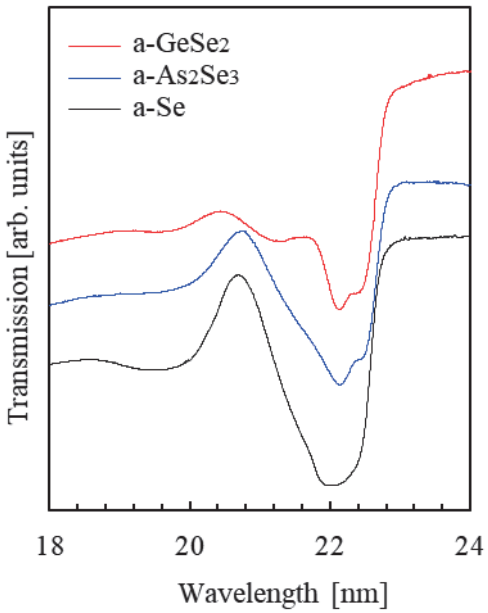

Fig. 1. VUV transmission spectra of amorphous $GeSe_2$, amorphous As_2Se_3, and amorphous Se thin films.

[1] Ke. Tanaka, Rev. Solid State Sci. **4** (1990) 641.
[2] K. Hayashi, UVSOR Activity Report **50** (2022) 152.
[3] J. Bordas and J. B. West, Phil. Mag. **34** (1976) 501.

BL5B

Reflectance of La/B_4C Reflective Multilayers

T. Ejima[1,2], R. Nakamura[3] and T. Hatano[1,2]
[1]*SRIS &* [2]*IMRAM, Tohoku University, Sendai 980-8577, Japan*
[3]*Dept. Appl. Physics, Tohoku University, Sendai 980-8577, Japan*

A wavelength in the soft X-ray (SX) region around 6.x nm has been proposed as a candidate for next-generation semiconductor lithography [1]. In this wavelength range, light penetration is significantly limited, necessitating the use of reflective optics based on multilayer structures. These multilayers typically consist of alternating layers of two materials that exhibit both low absorption and a large difference in refractive index. Ensuring a sharp interface between these materials is paramount for preserving the index contrast. Given that the periodic thickness of the film is approximately half the target wavelength at near normal incidence, the influence of the interface becomes increasingly critical as the wavelength decreases.

Currently, LaN/B-based multilayers are among the most reflective near 6.x nm [1]. These are fabricated via reactive magnetron sputtering using N_2 gas. However, the reactive gas can also interact with B, forming BNx compounds at the LaN/B interface and thereby degrading reflectance. To address this issue, we investigated La/B_4C multilayers as a promising alternative that eliminates the need for reactive sputtering (Fig. 1). B_4C has a negative enthalpy of formation and is thermodynamically stable in its standard state [2], while La is defined in its most stable phase [3]. This suggests that the La/B_4C pair can form stable, sharply defined interfaces in thin-film form.

The multilayers were deposited using ion beam sputtering at acceleration voltages of 1.0, 1.5, and 2.0 kV. X-ray reflectometry revealed the corresponding period lengths to be 3.63 nm, 3.52 nm, and 3.80 nm, respectively, indicating that ion energy primarily affects the interfacial structure.

Figure 2 presents preliminary reflectance spectra near 6.x nm for samples deposited at 1.0 kV and 2.0 kV. The observed variations in reflectance are believed to result from differences in interface quality induced by the ion energy.

In summary, the La/B_4C multilayer system demonstrates promising reflectance performance without the complications associated with reactive sputtering. The correlation between ion energy and interface sharpness highlights a critical parameter for further optimization. Ongoing and future work will aim to systematically improve reflectance by refining deposition conditions and enhancing interface control in La-based multilayers.

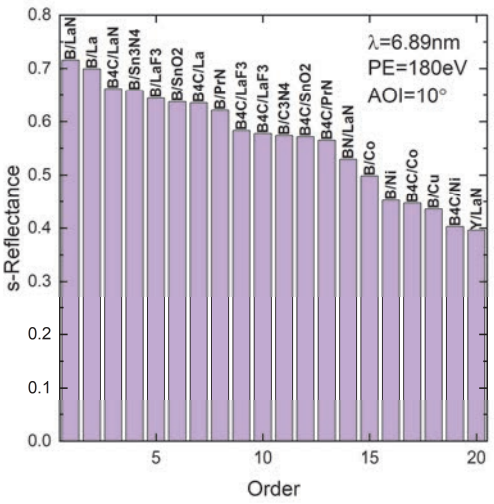

Fig. 1. A comparison of s-polarized reflectance for each material pair, with the horizontal axis indicating rank and the vertical axis displaying s-polarized reflectance. It is notable that the maximum value is B/LaN.

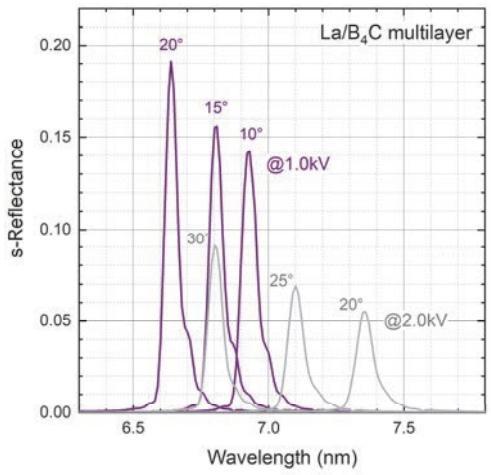

Fig. 2. A comparison of s-polarized reflectance for La/B_4C multilayers measured in the near normal incidence geometry (AOI: 10° – 30°).

[1] D. Kuznetsov *et al*., Opt. Lett. **40** (2015) 3778.
[2] M. W. Chase Jr., J. Phys. Chem. Ref. Data, Monograph **9** (1998) 1.
[3] R. H. Schumm, D. D. Wagman, S. Bailey, W. H. Evans, and V.B. Parker in National Bureau of Standards (USA) Technical Notes, (1973) 270.

Conduction Band of Single Crystal Graphite Embedded in Photoemission Energy-Loss Electrons Visualized by Photoelectron Momentum Microscope

F. Matsui[1], R. Sagehashi[2] and Y. Sato[1]

[1]*UVSOR Synchrotron Facility, Institute for Molecular Science and School of Physical Sciences, The Graduate University for Advanced Studies (SOKENDAI), Okazaki 444-8585, Japan*

[2]*Department of Photo-Molecular Science, Institute for Molecular Science, Okazaki 444-8585, Japan*

The interaction of secondary electrons (SEs) with the conduction band in the photoemission process reduces the emission intensity into the vacuum and produces a negative conduction band pattern contrast [1,2]. This process is very similar to the generation of negative photoelectron diffraction patterns observed in the angular distribution of energy-loss electrons accompanying core-level photoelectron excitation [3]. This means that the same setup as a standard photoelectron spectroscopy system for the characterization of occupied states can be used to visualize the electron-unoccupied conduction band.

Photoelectron momentum microscopy is a suitable system to measure comprehensive band dispersion structure in multiple dimensions (*kx*, *ky*, *kz*, *E*). Here we show that the conduction band of graphite are embedded in the angular and energy distribution of SEs. In addition, the experiment was performed in single-bunch mode, which has a photon flux one order of magnitude lower than the conventional multi-bunch mode. Since the SE intensity is very strong, low photon flux conditions are rather suitable for measuring such bulk crystal conduction band dispersion.

Figure 1(a) shows the overall dispersion of the valence band of graphite. Darker features correspond to directions of larger photoelectron signals. The photon energy was set to 68 eV to match the bulk L symmetry point. The selective detection of photo-electrons from a terrace with a single type of termination confirms that L and L' are not equal, as shown in Figure 1(b) [4]. At the binding energy (BE) of 2.8 eV, the triangles around point K touch each other at point L but are separated at point L'.

Figure 1(c) shows the momentum- resolved kinetic energy distribution of SE electrons. The unoccupied band dispersion appeared as a negative contrast due to the photoelectron absorption process by the conduction band states. Figure 2(d) shows a series of angular patterns at several kinetic energies. The key finding here is that most of the patterns appear with six-fold symmetry, but at kinetic energies of about 20 eV, the patterns become three-fold symmetric. The mechanism by which the three-fold symmetric structure of the top surface of graphite affects the conduction band remains an open question.

[1] V. N. Strocov *et al.* Phys. Rev. B **63** (2001) 205108.
[2] T. Takahashi *et al.*, Phys. Rev. B **32** (1985) 8317.
[3] F. Matsui *et al*., J. Phys. Soc. Jpn. **81** (2012) 013601.
[4] F. Matsui and S. Suga, Phys. Rev. B **105** (2022) 235126.

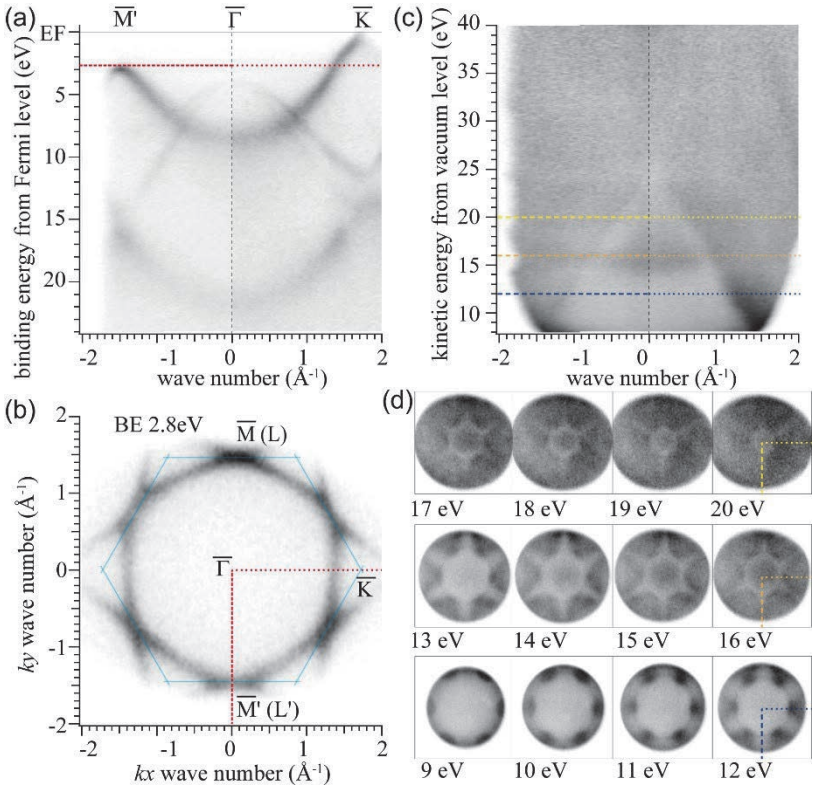

Fig. 1. (a) The overall dispersion of the valence band of graphite. Darker features correspond to directions of larger photoelectron signals. (b) Momentum distribution at the binding energy of 2.8 eV. A red line in (a) corresponds to that in (b). (c) The momentum-resolved kinetic energy distribution of SE electrons. The conduction band signature appears as a lighter grey contrast. (d) A series of SE momentum patterns at several kinetic energies. Note that at kinetic energies of 19 and 20 eV, the patterns appear as three-fold symmetric.

BL6U

Photoelectron Momentum Maps of MnPc on Single Crystal Graphite

R. Sagehashi[1], Y. Sato[2], F. Matsui[2] and S. Kera[1,2]
[1]*Department of Photo-Molecular Science, Institute for Molecular Science, Okazaki 444-8585, Japan*
[2]*UVSOR Synchrotron Facility, Institute for Molecular Science, Okazaki 444-8585, Japan*

Metal complex molecules form ligand fields, which resolve *d*-orbital degeneracy of their metal atoms. Metal-phthalocyanine (MPc) has planar structure and a transition metal atom is located at the center (shown in the inset of Fig. 1). Since MPc molecules are stacked on top of each other via π-π interaction, the ligand field is also formed between layers [1]. Therefore, the electronic and spin state is affected by the film formation significantly.

In this study, we investigated the influence of Mn-phthalocyanine (MnPc) adsorption and film formation on its electronic state by using photoelectron momentum microscopy (PMM) at BL6U. Here, single crystal graphite (SCG) for the substrate was cleaved in vacuum ($< 9.90\times10^{-8}$ Pa). MnPc was in-situ deposited ca. 6.0 Å by deposition rate of 0.30 Å/min measured by quartz crystal microbalance. In this PMM experiment, incoming light had photon energy of 54.0 eV and incident with 68° to the surface normal. The sample temperature was controlled by liquid helium during the measurements.

Figure 1 shows photoelectron spectroscopy (PES) spectra on cleaved SCG and MnPc/SCG taken at room temperature (RT) and ca. 10 K. Peak A is derived from Pc π-orbital as found for other MPcs. Peak B is uniquely observed for the MnPc as the highest occupied molecular orbital (HOMO) which is contributed strongly from Mn 3*d*-orbital. These peaks are shifted and become sharper at 10 K. Figures 2 (a-c) are the momentum maps at the energy of peak A (ΔE = 0.20 eV). In Fig. 2 (a), the intensity pattern from the SCG π-bands can be confirmed clearly. By adsorption of MnPc, the ring-like pattern along the π-bands of SCG at RT appeared (Fig. 2 (b)). On the other hand, the momentum map of MnPc/SCG at 10 K (Fig. 2 (c)) shows another intensity patterns with several lobes, where the faint ring-like pattern of the RT sample is superimposed. According to DFT calculations on MPc, the momentum map at HOMO shows the specific intensity patterns reflected C_{4v} symmetry [2]. Ring-like pattern suggests that π-orbital planes of the MnPc molecules are not ordered azimuthally on SCG at RT, then the several molecules make stable structure upon the cooling to give a specific lobe pattern. The presence of some disordered domains is indicated by the faint ring-like pattern at 10 K.

Additionally, another intensity pattern by six lobes appeared inside of the ring-like pattern at 10 K. Figures 2 (d-f) show band distribution maps corresponding to the momentum maps, respectively. In the distribution map of MnPc/SCG at 10 K (Fig. 2 (f)), another band dispersion can be confirmed inside of SCG π-bands and the value of k_x is coincident with the six-lobe pattern in the momentum map.

Since the interaction between MnPc and graphite is so weak [3], it is unlikely that a chemical change occurred between them. It is possible to consider that the appearance of band dispersion is due to phonon scattering at MnPc layers and derived from SCG π-bands. The reason for the appearance at 10 K may be due to the formation of oriented MnPc layers by cooling. These results lead to deeper understanding of weak molecule-substrate interactions.

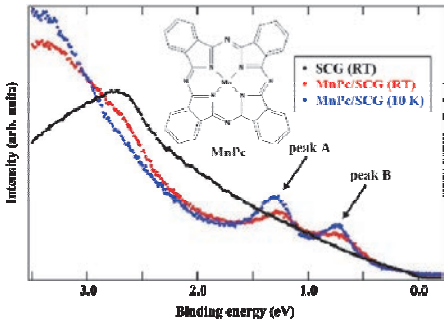

Fig. 1. Photoelectron spectra on the cleaved SCG and MnPc/SCG integrated over the whole angle. The structural formula of MnPc is shown in the inset.

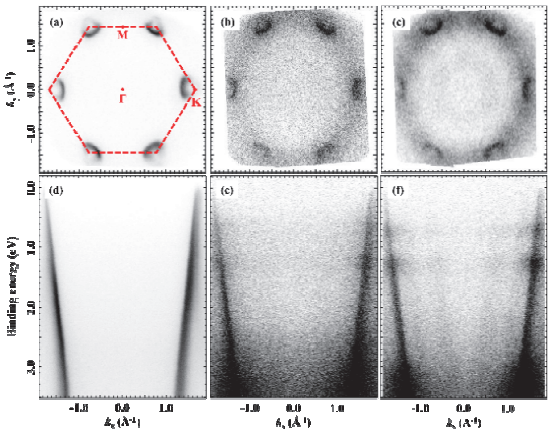

Fig. 2. (a-c): Momentum maps at peak A in Fig. 1. (a): Cleaved SCG and schematic image of hexagonal Brillouin zone. (b): MnPc/SCG at RT. (c): MnPc/SCG at 10 K. (d-f): Band distribution maps integrated over the range of k_y = (0.0±0.3) Å^{-1}. (d): Cleaved SCG. (e): MnPc/SCG at RT. (f): MnPc/SCG at 10 K.

[1] K. Nakamura *et al.*, Phys. Rev. B **85** (2012) 235129.
[2] D. Lüftner *et al.*, J. Elec. Spec. **195** (2014) 293.
[3] C. Isvoranu *et al.*, J. Chem. Phys. **131** (2009) 214709.

BL6U

Imaging the Domain Boundary of Ir(111) Thin Films by Momentum-selective PEEM Using Photoelectron Momentum Microscope

E. Hashimoto[1], H. Kurosaka[1], Y. Nishio[1], K. Hagiwara[2], F. Matsui[2] and S. Koh[1]

[1]*Department of Electrical Engineering and Electronics, College of Science and Engineering, Aoyama Gakuin University, 5-10-1 Fuchinobe, Chuo-ku, Sagamihara, Kanagawa 252-5258, Japan*

[2]*UVSOR Synchrotron Facility, Institute for Molecular Science, Okazaki 444-8585, Japan*

Iridium (Ir) is a transition metal belonging to the platinum elements group. Ir(111) is promising as a substrate for graphene growth by chemical vapor deposition (CVD). In addition, Ir(001) is used as a growth substrate for CVD diamond and a spin filter with high spin detection efficiency in spin-resolved photoemission spectroscopy. It is desired to establish methods for fabricating high quality Ir thin films at a few Å thick near the surface that can replace expensive bulk-single-crystals and methods for their characterization. In this study, we deposited Ir(111) thin films with high single-crystallinity by molecular beam epitaxy (MBE) and visualized the domain structure by momentum selective photoelectron emission microscopy (PEEM) using photoelectron momentum microscope [1,2].

We deposited Ir(111) thin films on α-Al_2O_3(0001) substrates by MBE method. First, the low-temperature buffer layer was deposited with the temperature of the substrate holder set at 500°C for 180 min. Then, the temperature of the sample holder was raised to 950°C, and the Ir(111) thin films were deposited for 120 min. By deposition for a total of 300 min, thin films with a thickness of 60 nm were grown. Afterwards, Ir(111) thin films were annealed under H_2 atmosphere at 1000°C for 60 min. Figures 1(a) and (b) show the XRD diffraction for the Ir layers on α-Al_2O_3(0001). Diffraction peaks caused by Ir(111) and α-Al_2O_3(0001) were observed in the $2\theta/\omega$ profile (Fig.1(a)). The XRD pole figure along Ir[111] is shown in Fig.1(b). The observed Bragg peaks displayed 6-fold symmetry, whereas the ideal Bragg peaks for Ir{111} exhibit 3-fold symmetry, thus indicating that Ir(111) contained twin domains.

Figures 2(a)-(c) show the band structures of Ir(111) thin films at Fermi energy by momentum-resolved photoelectron spectroscopy (MRPES). The field of view of MRPES is φ5 μm The photon energy was set to 100 eV. As shown in Fig. 2(a), we observed a 3-fold symmetry pattern of Ir. At the different measurement point 100 μm apart from the initial point, a 6-fold symmetry pattern corresponding to a domain boundary was observed (Fig.2(b)). With further movement of the measurement point, a 3-fold symmetry pattern rotated by 180 degrees from the 3-fold symmetry pattern at the initial point was observed (Fig.2(c)).

Momentum-selective PEEM images were acquired by inserting the contrast aperture into momentum space with the strongest photoelectron intensity in the MΓM direction ($E = E_F$ - 1 eV, $k_x \simeq 0$ Å^{-1}, $k_y \simeq 1$ Å^{-1}, in Fig. 2(a)). Without inserting the aperture, the PEEM image without contrast was obtained, which did not reflect the domain structure, as shown in Fig.3(a). In Fig. 3(b), when the aperture was inserted, we observed that the bright region corresponded to the domain with band structure, as shown in Fig.2(a). On the contrary, when an aperture is inserted in the domain with Fig. 2(c), a PEEM image with inverted contrast can be imaged, as shown in Fig. 3(c). Repeating similar PEEM measurements in different regions, found that unidirectional domains exist over several hundred μm × several hundred μm. We successfully observed twin-domain structures with no chemical shifts and only geometric differences in band structure using momentum-selective PEEM measurements.

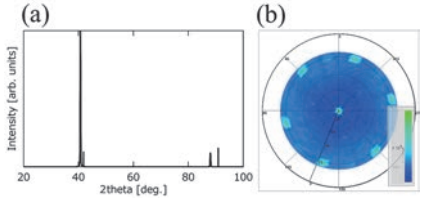

Fig. 1. (a) 2θ/ω profile and (b) pole figure of Ir(111) thin films deposited by MBE.

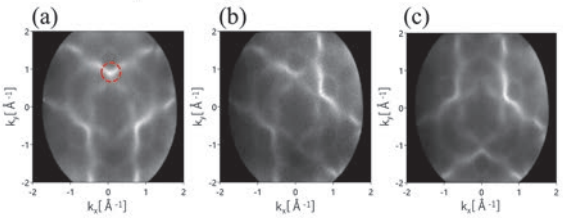

Fig. 2. The band structures of Ir(111) at Fermi energy. The observation point of (b) was moved 100 μm from (a), and (c) was moved 100 μm from (b).

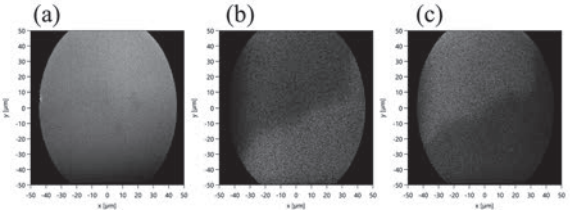

Fig. 3. PEEM images of Ir(111) thin films. (a) without inserting aperture, (b) and (c) with inserting aperture.

[1] F. Matsui *et al*., J. Phys. Soc. Jpn. **91** (2022) 097403.
[2] F. Matsui *et al*., Rev. Sci. Instrum. **94** (2023) 083701.

III-4

BL6B

Probing Molecular Vibration Dynamics of Layered Borophene Oxide Thin Films using *In-Situ* Variable-Temperature Infrared Spectroscopy

K. Kaminaga[1], K. Sasaki[1], H. Murakami[1], F. Teshima[2], A Kikuchi[1], K. Tanaka[2], S. Maruyama[1] and Y. Matsumoto[1]

[1]*Department of Applied Chemistry, Tohoku University, Sendai 980-8579, Japan*

[2]*Institute for Molecular Science (IMS), National Institutes of Natural Sciences, 38 Nishigonaka, Myodaiji, Okazaki 444-8585, Japan*

Liquid crystals represent a distinctive mesophase exhibiting properties characteristic of both fluids and crystalline solids, and they are well-established as functional materials in electronic display technologies. While the field has historically been dominated by organic compounds due to their molecular flexibility, the synthesis of inorganic liquid crystals has proven challenging, largely attributed to the rigidity inherent in inorganic bonding. Nevertheless, the development of stable inorganic liquid crystals holds significant promise for applications in extreme environments where organic materials often prove inadequate.

A key advancement occurred in 2022 with the report of layered borophene oxide (BoL), synthesized from potassium borohydride (KBH_4) [1]. This material undergoes a structural phase transition to a liquid crystalline state at approximately 120°C, a process associated with dehydration reactions [2]. Notably, this liquid crystalline phase can be rendered metastable at ambient temperature through supercooling. Recognizing the potential for semiconductor applications, our research group has developed a vapor-phase synthesis protocol for BoL thin films using infrared laser deposition. This method involves the selective oxidation of KBH_4 precursor molecules, catalyzed by acetonitrile vapor under vacuum conditions (Fig.1 inset).

Previous infrared spectroscopic studies on bulk BoL characterized the modulation of O-H and B-O vibrational modes during the transition between crystalline and liquid crystalline phases [2]. However, despite X-ray diffraction analyses confirming the reversibility of this phase transition in thin films, the specific molecular-level structural alterations occurring within these films remain insufficiently understood.

To address this gap, the present investigation utilized temperature-variable Fourier-transform infrared (FT-IR) spectroscopy to analyze BoL thin films deposited on double side polished Si substrates. FT-IR spectroscopy was performed with a FT-IR microscope (JASCO, IRT-7000) at beamline BL6B. Infrared radiation was directed through a Michelson-type interferometer (JASCO, FT/IR-6100). The measurements were conducted in a reflectance configuration, with the incident IR beam aligned perpendicular to the surfaces of samples. To mitigate atmospheric interference, the IR absorbance spectra were derived by normalizing the reflectance spectra of the KBH_4 samples against that of a gold (Au) film. Measurements performed under atmospheric conditions successfully detected the characteristic B-O (~1500 cm^{-1}) and O-H (~3000 cm^{-1}) vibrational modes, thereby confirming the successful synthesis of the target thin films (Fig.1). On the other hand, attempts to perform measurements under vacuum were hindered by instrumental difficulties related to optical alignment.

In conclusion, future experimental work will focus on implementing refined optical axis calibration procedures to enable reliable vacuum-environment FT-IR measurements. This refinement is crucial for facilitating comprehensive in-situ observation of the temperature-dependent phase transition, free from atmospheric interference. Such optimized methodology will permit a systematic vibrational spectroscopic analysis of the structural reversibility between the crystalline and liquid crystalline phases at the molecular level.

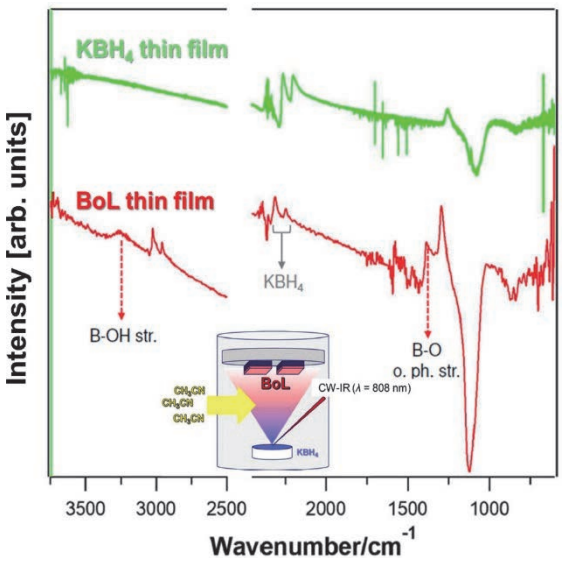

Fig. 1. IR spectra of KBH_4 thin film (green) and BoL thin film (red) under atmospheric conditions. Inset: Schematic of the experimental setup for BoL thin film growth.

[1] T. Kambe *et al*., J. Am. Chem. Soc. **141** (2019) 12984.
[2] T. Kambe *et al*., Nat Commun. **13** (2022) 1037.

Electronic Structure Study of Topological Materials $Ge_2Bi_2Te_5$ and $Ge_3Bi_2Te_6$

Y. Dai[1], X. M. Ma[1] and C. Liu[1]
[1]*Southern University of Science and Technology (SUSTech), Shenzhen, Guangdong 518055, China*

The $MnBi_2Te_4(Bi_2Te_3)_n$ compounds, with $MnBi_2Te_4$ being a prototypical member, have been established as model systems of intrinsic magnetic topological insulators [1-3]. The characteristic van der Waals structure of $MnBi_2Te_4$ comprises alternating Te-Bi-Te-Mn-Te-Bi-Te layers with single Mn layers per unit cell, supporting antiferromagnetic (AFM) ordering below 24 K and manifesting intricate magneto-topological coupling [4, 5]. However, a fundamental constraint arises from the limited magnetic layer density: the single-Mn-layer configuration leads to weak interlayer magnetic coupling and suppresses Neel temperatures, hindering potential applications.

Recent theoretical works propose that structural engineering through magnetic layer stacking – as exemplified in $Mn_2Bi_2Te_5$ and $Mn_3Bi_2Te_6$ derivatives – could enhance magnetic ordering temperatures [6, 7]. On one hand, $Mn_2Bi_2Te_5$ has been predicted to host a *dynamic axion insulator* state, offering an unprecedented platform for exploring topological electromagnetic responses [6]. On the other hand, first-principles calculations reveal a magnetic-order-dependent topological phase transition in $Mn_3Bi_2Te_6$, with the AFM configuration remaining topologically trivial while the ferromagnetic (FM) ordering induces nontrivial topology [7]. Despite these compelling predictions, experimental verification remains elusive due to formidable single-crystal growth challenges.

To circumvent the synthesis bottleneck, we adopt a chemical substitution strategy leveraging the structural stability of isostructural germanium analogs $Ge_2Bi_2Te_5$ and $Ge_3Bi_2Te_6$ [8, 9]. Through progressive substitution of Ge with Mn in $(Ge_{1-x}Mn_xTe)_mBi_2Te_3$ (m = 2, 3), we aim to engineering systems combining robust magnetic ordering with topological functionality.

Our experimental investigation combines angle-resolved photoemission spectroscopy (ARPES) measurements at UVSOR BL7U with systematic Mn doping. Initial characterization of parent compounds $Ge_2Bi_2Te_5$ (Fig. 1a) and $Ge_3Bi_2Te_6$ (Fig. 2a) established baseline electronic structures. Subsequent doping studies focus on nominal Mn concentration of 20% and 30% in $(Ge_{1-x}Mn_x)_2Bi_2Te_5$, and 30% in $(Ge_{1-x}Mn_x)_3Bi_2Te_6$.

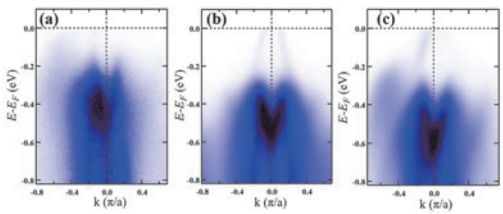

Fig. 1. Band evolution on $(Ge_{1-x}Mn_x)_2Bi_2Te_5$ with different nominal Mn doping levels x = 0 (a), x = 0.2 (b) and x = 0.3 (c) ($h\nu$ = 20 eV). The measurement direction is Γ-M for (a) and (c), and Γ-K for (b). As x increases, the Fermi level moves upward.

ARPES data reveal progressive Fermi level upshifting with increasing Mn content, indicative of n-type dosage. The $(Ge_{1-x}Mn_x)_3Bi_2Te_6$ system manifests electronic features suggestive of hole-doped analogs to its m = 2 counterpart. While both systems preserve threefold rotational symmetry in constant-energy contours (Fig. 3d), subtle differences in their band dispersion await theoretical interpretation.

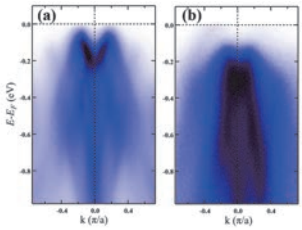

Fig. 2. Band evolution on $(Ge_{1-x}Mn_x)_3Bi_2Te_6$ with different nominal Mn doping levels x = 0 (a) and x = 0.2 (b) ($h\nu$ = 20 eV). The measurement direction is Γ-K for (a) and Γ-M for (b). As x increases, the Fermi level moves upward.

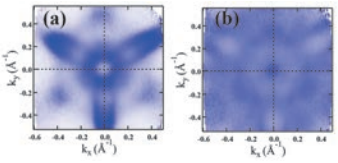

Fig. 3. ARPES constant-energy contour of $(Ge_{0.8}Mn_{0.2})_2Bi_2Te_5$ with $h\nu$ = 21 eV. The binding energy of each penal is 0.25 eV (a) and 1.35 eV (b).

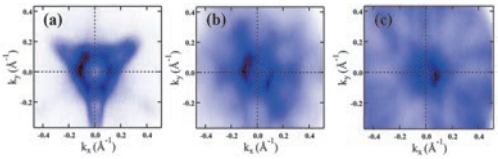

Fig. 4. ARPES constant-energy contour of $Ge_3Bi_2Te_6$ with with $h\nu$ = 19 eV. The binding energy of each penal is 0.05 eV (a), 0.35 eV (b) and 1.45 eV (c).

[1] D. Zhang *et al*., Phys. Rev. Lett. **122** (2019) 206401.
[2] Klimovskikh *et al*., npj Quantum Mater. **5** (2020) 54.
[3] H. Deng *et al*., Nat. Phys. **17** (2021) 36.
[4] J. Zhang *et al*., Chin. Phys. Lett. **37** (2020) 077304.
[5] A. Gao *et al*., Nature **595** (2021) 521.
[6] J. Zhang *et al*., Chin. Phys. Lett. **37** (2020) 077304.
[7] W. Wu *et al*., J. Phys.: Condens. Matter **36** (2024) 125701.
[8] Matsunaga *et al*., Acta Cryst. B **63** (2007) 346.
[9] L. E. Shelimova *et al*., Inorganic Materials **36** (2000) 235.

BL7U

Electronic State Analysis of Bcc-Cu Thin Film on FeCo/MgO(100)

S. Takezawa[1,2] and N. Nagamura[1,2,3]

[1]*Graduate School of Advanced Engineering, Tokyo University of Science, Tokyo 125-8585, Japan*
[2]*Center for Basic Research on Materials, National Institute for Materials Science, Tsukuba 305-0003, Japan*
[3]*Research Institute of Electrical Communication, Tohoku University, Sendai 980-0812, Japan*

Copper typically crystallizes in a face-centered cubic (fcc) structure as its most stable phase. However, in nanocrystalline systems or certain ultrathin films, it can adopt a metastable body-centered cubic (bcc) structure[1,2]. Notably, bcc-Cu/FeCo multilayers have been reported to exhibit high magnetoresistance (MR) ratios in three-layer giant magnetoresistance (GMR) devices[3]. This enhancement in MR ratio is strongly influenced by modulation of the electronic states at the Cu/FeCo interface, which arises from the formation of the metastable Cu phase. Nevertheless, there have been no experimental reports directly observing the electronic structure of bcc-Cu and its thickness-dependent modulation. This is primarily due to the difficulty in fabricating clean bcc-Cu(001) surfaces using conventional sputtering techniques.

In this study, we performed angle-resolved photoemission spectroscopy (ARPES) measurements on bcc-Cu/FeCo/MgO(001) thin films grown *in-situ* by molecular beam epitaxy (MBE) at the UVSOR BL7U beamline. The MgO(001) substrates were annealed at 500 °C for 60 minutes to clean the surface. The FeCo underlayer was deposited at a substrate temperature of 300 °C. The epitaxial growth of the FeCo layer and the cleanliness of the FeCo(001) surface were confirmed by low-energy electron diffraction (LEED) measurements (Fig. 1). Subsequently, a 1 nm-thick Cu layer was deposited at room temperature, and the formation of a clean bcc-Cu(001) surface was confirmed by LEED (Fig. 1). For comparison, an additional 20~ nm of Cu was deposited at room temperature to intentionally induce a structural transition to fcc-Cu, thereby fabricating fcc-Cu/FeCo/MgO(001) thin films. ARPES measurements were performed immediately after each deposition step.

Figure 2 (c)-(e) shows the ARPES results for FeCo(001), bcc-Cu(001), and fcc-Cu(001). ARPES measurements of FeCo ware performed at T = 250 K, ARPES measurements of bcc-Cu and fcc-Cu were performed at T = 15 K. Upon Cu deposition, a flat band attributed to Cu 3*d* electrons appeared near a binding energy = 2–3 eV. Furthermore, the electronic structure of Cu was found to be modulated as the film thickness increased. This modulation is considered to reflect the structural phase transition from the metastable bcc phase to the stable fcc phase. In addition, the spectra exhibited photon energy dependence, suggesting the presence of a three-dimensional electronic structure. These results not only provide fundamental insights into the electronic properties of bcc-Cu but also indicate the potential for tuning the electronic structure of Cu through thickness modulation.

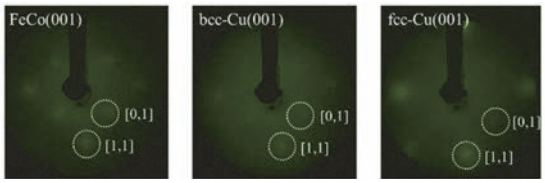

Fig. 1. LEED patterns of FeCo(001), bcc-Cu(001), fcc-Cu(001). Clean surfaces are observed respectively. All images are taken at incident electron beam energy = 210 eV.

[1] H. Li *et al*, Phys. Rev. B, **43**, (1991) 8.
[2] Z. Wang *et al*, Phys. Rev. B, **35**, (1987) 17.
[3] K. B. Fathoni *et al*., APL Mater., **7**, (2019) 111106.

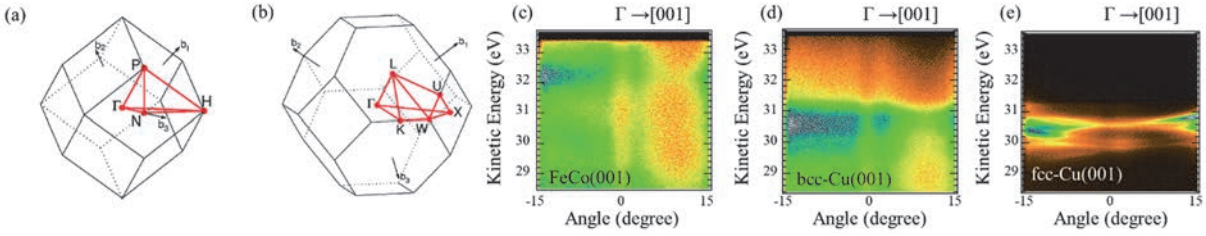

Fig. 2. (a) Brillouin zone of bcc lattice. (b) Brillouin zone of fcc lattice. (c)-(e)ARPES spectra of each sample along [001] axis. All spectra are measured at hν = 38 eV. Modulation of electronic states depending on the thickness of the Cu film was observed.

BL7U

Thin-Film Growth and Electronic Structure Study on YbSb/GaSb(110)

Y. Chen[1], T. Nakamura[2,1], R. Ichikawa[1], H. Yamaguchi[1], K. Nishihara[1], K. Tanaka[3] and S. Kimura[2,1,4]

[1]*Department of Physics, Graduate School of Science, The University of Osaka, Toyonaka 560-0043, Japan*
[2]*Graduate School of Frontier Biosciences, The University of Osaka, Suita 565-0071, Japan*
[3]*UVSOR Synchrotron Facility, Institute for Molecular Science, Okazaki 444-8585, Japan*
[4]*Department of Material Molecular Sciences, Institute for Molecular Science, Okazaki 444-8585, Japan*

Rare-earth mono-pnictide (*REPn*: *RE* = rare-earth element, *Pn* = pnictogen (Group V element)) exhibits a variety of magnetic properties, such as extreme magnetoresistance (XMR) reaching up to more than 10^6 % of the value at zero field [1], and a complicated magnetic phase transition in CeSb [2]. These characteristic physical properties originate from the hybridization between localized 4*f* orbitals in rare-earth elements and *p* orbitals in pnictogen elements, namely *p-f* mixing [3]. Recently, the existence of spin-polarized surface states in some *RE*Sbs and *RE*Bis [4] and the high-quality epitaxial thin-film grown by a molecular beam epitaxy (MBE) method were reported [5]. These novel studies lead us to anticipate possibilities as potential applications in spintronics devices. Meanwhile, despite the intense study on the *REPn* family, the knowledge of Yb mono-pnictides, such as YbSb, is still limited because of the difficulty in bulk single-crystal synthesis due to the high vapor pressure of Yb. We are focusing on the MBE growth and the electronic structure study on YbSb thin film. So far, we have tried the growth of YbSb thin film on the GaSb(001)-c(2×6) surface cleaned by Ar^+ sputtering and annealing. The obtained thin film shows an unexpected (2×1) reconstructed surface and a Fermi surface with 2-fold rotational symmetry [6]. Here, we fabricated YbSb thin films on another GaSb surface (110) to understand the origin of the anisotropy of YbSb/GdSb(001)-c(2×6).

To clarify the role of the surface-preparing method, we used two cleaning methods; one is Ar^+ sputtering at the substrate temperature of 720 K for 30 minutes, and the other is direct cleaving along the (110) plane. Yb and Sb were co-evaporated onto the cleaned substrates at 570 K with the flux-rate ratio of Yb and Sb as 1:1.1. Figure 1 shows LEED patterns measured after the deposition of YbSb for ~15 ML. For the thin-film growth on both substrates, streaks along the [001] direction with the same spacing as the diffraction spots of GaSb(110) on the [$\bar{1}$10] direction are observed. This result suggests that the substrate-preparing method is not essential for the sample quality.

Electronic structures of the differently prepared samples were detected with a synchrotron-based ARPES measurement. In the ARPES measurement, no clear dispersion could be observed along the [001] direction because of the lack of the long-range periodicity. On the other hand, as shown in Fig. 2, three hole bands and one electron pocket can be easily identified along the [$\bar{1}$10] direction for both substrates. The obtained ARPES image is consistent with the band calculation of YbSb [7] and the ARPES results of other *RE*Sbs [8]. These results suggest that the fabricated films are YbSb with a 1D-like growth along the [$\bar{1}$10] direction. One possible explanation could be dimer rows along the [$\bar{1}$10] direction form a staircase-like structure with two different heights along the [001] direction. Another possibility is that the obtained Yb-Sb thin film is a different compound, $YbSb_2$, reported in a recent paper [9]. To clarify the origin of the 1D-like feature, further detailed studies on chemical composition and crystallography by XPS and XRD are needed.

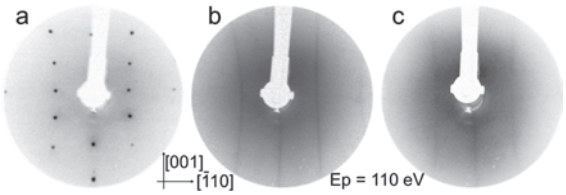

Fig. 1. LEED patterns of GaSb(110) cleaving surface (a), YbSb thin film growth on GaSb(110) substrates prepared by cleaving (b), and by Ar^+ sputtering (c), measured at 14 K.

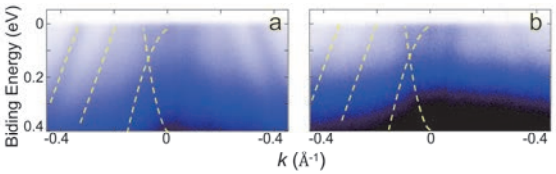

Fig. 2. ARPES intensity plots along the [$\bar{1}$10] direction and measured with 21-eV photons at 14 K of the YbSb thin-films growth on GaSb(110) substrates prepared by cleaving (a) and by Ar^+ sputtering (b).

[1] L. Ye *et al.*, Phys. Rev. B **97** (2018) 081108.
[2] J. Rossat-Mignod *et al*., J. Magn. Magn. Mater. **52** (1985) 111.
[3] H. Takahashi and T. Kasuya, J. Phys. C: Solid State Phys. **18** (1985) 2697, 2709, 2721, 2731, 2745, 2755.
[4] K. Kuroda *et al*., Phys. Rev. Lett. **120** (2018) 086402.
[5] S. Chatterjee *et al*., Phys. Rev. B **99** (2019) 125134.
[6] Y. Chen *et al*. UVSOR Activity Report **51** (2024) 164.
[7] X. Duan *et al*., Commun. Phys. **1** (2018) 71.
[8] P. Li *et al*., npj Quantum Mater. **8** (2023) 22.
[9] R. Dhara *et al*., Phys. Rev. Mater. **9** (2025) 034801.

BL7U

Observation of Electronic Structure of Chiral Magnet $GdNi_3Ga_9$ by ARPES

Y. Tanimoto[1], Y. Nakashima[1], H. Sato[2], K. Tanaka[3], S. Nakamura[4] and S. Ohara[4]
[1]*Graduate School of Advanced Science and Engineering, Hiroshima University, Higashi-Hiroshima 739-8526, Japan*
[2]*Hiroshima Research Institute for Synchrotron Radiation Science, Higashi-Hiroshima 739-0046, Japan*
[3]*UVSOR Synchrotron Facility, Institute for Molecular Science, Okazaki 444-8585, Japan*
[4]*Graduate School of Engineering, Nagoya Institute of Technology, Nagoya 466-8555, Japan*

Trigonal $GdNi_3Ga_9$ has a chiral crystal structure belonging to space group of *R*32 (No. 155) [1] and is of interest as a 4*f* chiral metallomagnetic compound [2]. The localized Gd 4*f* spins are magnetically ordered below T_N=19.5 K, forming an antiferromagnetic structure in the *ab*-plane, and exhibiting left- or right-handed helimagnetism with a propagation vector $\boldsymbol{q}$=(0, 0, 1.485) [2]. Spin-polarized conduction electrons are thought to be responsible for this phenomenon. $GdNi_3Ga_9$ has the same crystal structure as $YbNi_3Al_9$, the first discovered 4*f* chiral metallomagnetic compound [3]. $YbNi_3Al_9$ exhibits helimagnetism with $\boldsymbol{q}$=(0, 0, 0.82) [4], while ferromagnetic order in the *ab*-plane, in contrast to $GdNi_3Ga_9$. Thus, a comparative study for $GdNi_3Ga_9$ is expected.

We have previously performed angle-resolved photoemission spectroscopy (ARPES) on $YbNi_3Al_9$ and observed five hole-like Fermi surfaces around the $\overline{\Gamma}$ point and one electronic-like Fermi surface around the $\overline{K}$ point [5]. In this study, we conducted ARPES on $GdNi_3Ga_9$ to investigate the Fermi surface and band structure of conduction electronic states near the Fermi level (E_F). The experiments were carried out at BL7U of UVSOR-III using an electron analyzer (A-1, MB-Scientific). Single crystals for the ARPES measurements were synthesized by the flux-method using gallium as the solvent [2] and were cleaved *in situ* under an ultrahigh vacuum of ~5×10^{-9} Pa.

Figures 1(a) and 1(b) present ARPES intensity plots of $GdNi_3Ga_9$ measured at $h\nu$=24 eV with *p*-polarized and *s*-polarized geometries, respectively, along the $\overline{\Gamma}$-$\overline{M}$ direction of the surface Brillouin zone. Measurements were performed at 7 K, below T_N. At least three hole-like bands were observed around the $\overline{\Gamma}$ point in Fig. 1(a). On the other hand, Fig. 1(b) clearly shows two hole-like bands crossing E_F at k_x=0.3 and 0.5 Å^{-1}, as well as a convex-upward band around the $\overline{\Gamma}$ point. The shape of the observed bands closely resembles those of $YbNi_3Al_9$ [5].

Figures 2(a) and 2(b) show the Fermi surfaces of $GdNi_3Ga_9$ measured at $h\nu$=24 eV and *T*=7 K with *p*-polarized and *s*-polarized geometries, respectively. In Fig. 2(a), at least three hole-like Fermi surfaces, corresponding to the bands in Fig. 1(a), exhibit an approximately six-fold symmetry. In Fig. 2(b), two hole-like Fermi surfaces are observed, and that around k_x=0.4 Å^{-1} appears three-fold symmetric. The hole-like Fermi surfaces of $GdNi_3Ga_9$ appear larger compared to those of $YbNi_3Al_9$.

We have also measured ARPES spectra at 25 K above T_N. A remarkable change in the shape of the bands was not detected.

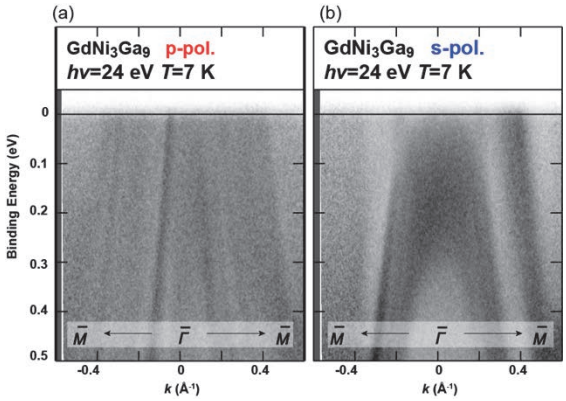

Fig. 1. ARPES intensity plots of $GdNi_3Ga_9$ measured along the $\overline{\Gamma}$-$\overline{M}$ direction at $h\nu$=24 eV and *T*=7 K with (a)*p*- and (b)*s*-polarized geometry.

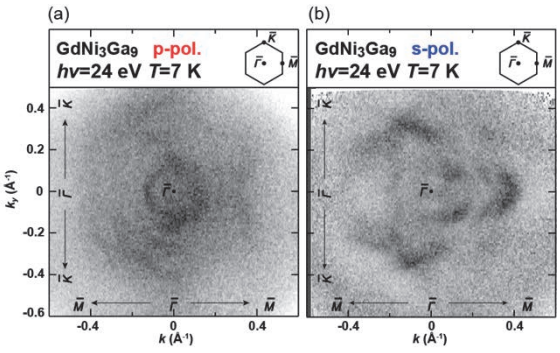

Fig. 2. The Fermi surfaces of $GdNi_3Ga_9$ measured at $h\nu$=24 eV and *T*=7 K with (a)*p*- and (b)*s*-polarized geometry.

[1] V. Topertser *et al*., Chem. Met. Alloys **12** (2019) 21.
[2] S. Nakamura *et al*., Phys. Rev. B **108** (2023) 104422.
[3] S. Ohara *et al*., JPS Conf. Proc. **3** (2014) 017016.
[4] T. Matsumura *et al*., J. Phys. Soc. Jpn. **86** (2017) 124702.
[5] Y. Tanimoto *et al*., in preparation.

BL7U

Photon Energy-dependent ARPES Study of Secondary Photoemission on $CaTiO_3$ and $BaTiO_3$

C.Z. Huang[1], C.Y. Hong[1], C.Y. Jiang[1,2], X.N. Zheng[1,2] and R.-H. He[1]
[1]*School of Science, Westlake Institute for Advanced Study, Westlake University, Hangzhou 310064, China*
[2]*Department of Physics, Fudan University, Shanghai 200433, China*

The discovery of the anomalous photocathode quantum material $SrTiO_3$ (STO) has garnered significant interest, yet the mechanism behind its extraordinary properties remains unclear[1]. Recently, a theoretical model introducing a novel Auger process that recycles secondary electrons and induces the emission of tertiary electrons has been proposed to explain the intense coherent photoemission in STO[2]. This model also predicts other perovskite oxides as candidate photocathode quantum materials and calls for further explorations.

As a technique that can directly probing the electronic structure of materials, Angle-resolved photoemission spectroscopy (ARPES) serves as a powerful tool for studying and discovering novel quantum materials. Photon energy-dependent ARPES measurements on STO have revealed that the intensity of the coherence peak is influenced by the excitation photon energy, with a threshold beyond which the peak intensity increases significantly[3]. $CaTiO_3$ (CTO) and $BaTiO_3$ (BTO), as perovskite oxides, are predicted to exhibit secondary photoemission characteristics similar to those of STO. Investigations into these materials may offer valuable insights into the mechanism underlying the exotic properties of these quantum materials.

Here, we report photon energy-dependent measurements on CTO and BTO thin films. The thin films were prepared by pulsed laser deposition and annealed at 1100-1200 ℃ for several hours to achieve clean surfaces for ARPES measurements. ARPES measurements were conducted at the BL7U beamline of UVSOR, utilizing photon energies ranging from 7.1 to 22 eV, with a sample temperature of 11 K.

Figure 1(a) shows the secondary photoemission spectrum (SPS) of CTO measured with photon energies ranging from 7.1 to 22 eV. The SPS peak at a kinetic energy of 4.3 eV remains nearly unchanged in position despite varying photon energy, while its intensity exhibits a clear photon energy dependence. As the photon energy increases to 8.1 eV, the peak intensity rapidly rises, reaching its maximum at a photon energy of 8.6 eV, and then begins to decrease. When the photon energy exceeds 12 eV, the peak intensity stabilizes.

For BTO, the variation of SPS peak intensity at a kinetic energy of 3.6 eV with photon energy follows a trend similar to that of CTO, exhibiting a threshold of 8.1 eV, a maximum of 8.8 eV, and stabilization above 12 eV.

The photon energy dependence of SPS peak intensity in CTO and BTO closely resembles that of STO, indicating a common origin for the anomalous secondary photoemission in these materials. Further investigations, such as examining the film thickness-dependence of SPS peak intensity, may provide more insights for understanding and utilizing these novel quantum materials.

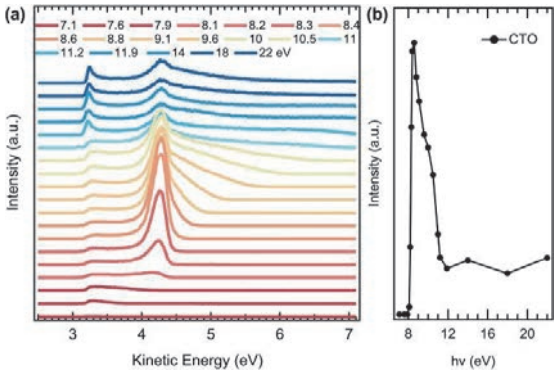

Fig. 1. (a) The secondary electron emission spectra of CTO measured with different photon energies. (b) The intensity of the peak at 4.3 eV as a function of photon energy.

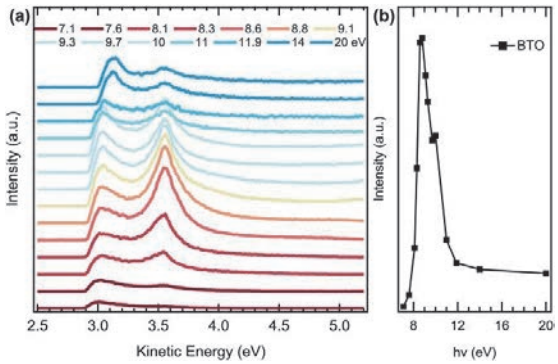

Fig. 2. (a) The secondary electron emission spectra of BTO measured with different photon energies. (b) The intensity of the peak at 3.6 eV as a function of photon energy.

[1] C. Hong *et al*., Nature **617** (2023) 493.
[2] M. Matzelle *et al*., arXiv:2405.06141 (2024).
[3] C. Hong *et al*.UVSOR Activity Report **51** (2023) 162.

BL7B

Polarization Dependence of Solid-Liquid Interfaces Probed by Attenuated Total Reflectance Ultraviolet (ATR-UV) Spectroscopy

I. Tanabe[1], T. Kakinoki[2] and K. Fukui[2]
[1]*Department of Chemistry, College of Science, Rikkyo University, Toshima 171-0021, Japan*
[2]*Department of Materials Engineering Science, Graduate School of Engineering Science, The University of Osaka, Toyonaka 560-8531, Japan*

Electric double-layer organic field-effect transistors (EDL-OFETs) have garnered significant interest for their ultra-low operating voltage (<1 V), which is markedly lower than that of conventional SiO_2-gated OFETs (>10 V). This reduced voltage is achieved through the formation of a high electric field within the electric double layer (EDL), which accumulates at the interface between the organic semiconductor and the electrolyte. Consequently, understanding and optimizing the organic semiconductor/electrolyte interface is crucial for the performance of EDL-OFETs.

Attenuated Total Reflection (ATR) spectroscopy is a useful method for studying interfaces. In particular, in the ultraviolet (UV) region, it provides valuable information about the electronic states of materials. We have previously utilized ATR-UV spectroscopy with a deuterium lamp as a light source to investigate the interfaces between organic semiconductors or metals and electrolytes [1, 2]. Through this approach, we have elucidated the electronic states of organic semiconductors and interfacial electrolytes depending on the applied voltage. While a deuterium lamp emits unpolarized light, the use of polarized light is expected to provide insights into the orientation of organic semiconductors and interfacial electrolytes. Therefore, in this study, we aimed to develop a new spectroscopic system utilizing polarized light obtained from BL7B at UVSOR.

A thin film of C9-DNBDT-NW (Figure 1a), a material reported to exhibit excellent mobility, was deposited onto a sapphire ATR prism and measured using ATR setup. By adjusting the orientation of the prism relative to the incident light, the polarization characteristics of the spectra were investigated. The results, shown in Figures 1b and 1c, reveal a clear polarization dependence. As shown in Figure 1b, *s*-polarized incident light produced distinct absorption peaks within the 200–500 nm range, whereas *p*-polarized light exhibited no such prominent features(Figure 1c).

Figures 1d and 1e illustrate the polarization-dependent absorption spectra of C9-DNBDT-NW, as calculated using time-dependent density functional theory (TD-DFT). The results indicate that along the x-axis (Figure 1d), multiple strong absorption features were predicted, whereas along the z-axis, almost no absorption was observed. Considering the experimental results, it is suggested that this thin film is structured with the x-axis oriented perpendicularly to the substrate.

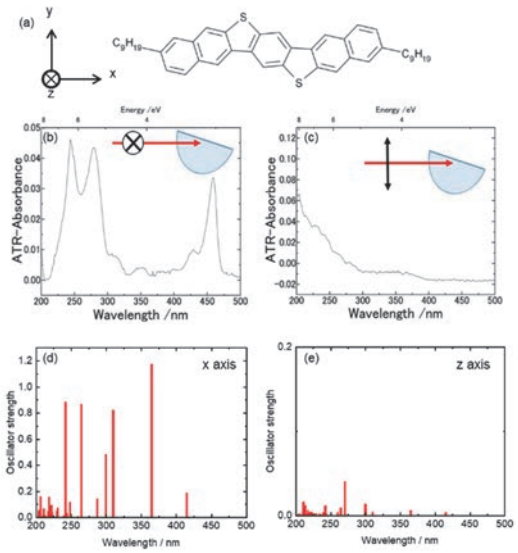

Fig. 1. (a) The structural formula of C9-DNBDT-NW. (b, c) Polarization dependence of ATR spectra of C9-DNBDT-NW on a sapphire prism. (d, e) Calculated vertical transitions along (d) x- and (e) z-axis of a C9-DNBDT-NW molecule.

Thus, polarization-dependent ATR spectroscopy enables the determination of the molecular orientation in organic thin films deposited on a sapphire substrate. Additionally, a key feature of ATR spectroscopy in the ultraviolet region is its short probing depth, limited to tens of nanometers due to the penetration depth of the evanescent wave. Moreover, by adjusting the incident angle, this probing depth can be finely controlled on the nanometer scale. Further advancements in this technique are expected to enable the investigation of electrochemical responses and the organic semiconductor-electrolyte interface.

[1] I. Tanabe *et al.*, Anal. Chem. **91** (2019) 3436.
[2] I. Tanabe *et al.*, Commun. Chem. **4** (2021) 88.

UVSOR User 13